The Pennsylvania State University

The Graduate School

Department of Mechanical Engineering

EMISSION CHARACTERISTICS OF JP-8, JP-900, FISCHER-TROPSCH (FT) AND JP-8/FT BLENDS IN A MODEL GAS TURBINE COMBUSTOR

A Thesis in

Mechanical Engineering

by

Vickey Kalaskar

Submitted in Partial Fulfillment

of the Requirements

for the Degree of

Master of Science

Dec 2009

The thesis of Vickey Kalaskar was reviewed and approved* by the following:

Dr. Robert J. Santoro

George L. Guillet, Professor of Mechanical Engineering

Director of the Propulsion Engineering Research Center

Thesis Advisor

Dr. Thomas A. Litzinger

Professor of Mechanical Engineering

Director of Leonhard Center

Dr. Karen A. Thole

Professor of Mechanical Engineering

Head of the Department of Mechanical and Nuclear Engineering

*Signatures are on file in the Graduate School.

Abstract

The increasing usage of coal-based fuels in aviation turbines and fluctuating prices of the crude oil imports emphasizes the need to study and analyze alternate coal-based fuels like JP-900 and Fischer-Tropsch (FT), which can be obtained from nationally owned sources. Currently, JP-8 fuel is being used as an aviation fuel for the U.S. Air Force operations. The properties of JP-900 and FT need to be characterized and compared with JP-8 in order to determine their feasibility as the next generation aviation fuels. JP-900 is a coal-based fuel which has been developed to serve two purposes: providing propulsion energy and providing good heat sink capabilities. FT fuel, in contrast, is a clean burning fuel expected to produce very low pollutant emissions, soot and highly stable operation.

Gas turbine engines have temperature limitations. All efforts are being made to increase the operating pressure regimes of modern day combustors to improve overall combustion performance and achieve greater efficiencies. Increase in the operating pressures gives rise to higher adiabatic flame temperatures. High temperature is undesirable for the combustor linings and components downstream of the combustor, therefore, new methods are being developed to improve heat transfer from the combustor walls. A fuel with excellent heat sink capabilities can serve as a coolant for hot engine components. JP-900 exhibits good heat sink capability and oxidative stability at higher temperatures (900^0F). However, successful development of a versatile, multiple-use fuel must achieve the desired operational characteristics of high combustion efficiency,

excellent combustion stability, acceptable pollutant emission levels, and compatibility with current engine seals.

Current requirements of strict emissions standards and improved stability are major areas of concern with regards to the usage of alternative jet fuels. Combustion instability can have damaging effects on combustor components. These instabilities are closely tied to the combustion geometry, fuel injection, fuel/air mixing properties and heat release characteristics. Combustion instability, CO and NO_x emissions, and mean soot volume fraction vary with fuel composition. Therefore, changes in fuel composition may drastically affect the overall combustion and emission characteristics. These fuels would require a vigilant consideration through a well synchronized research program prior to being used in existing engines.

The current study investigates the feasibility of alternative coal-based jet fuels considering the combustion requirements of aviation turbines. JP-900, FT and (25/75), (50/50) JP-8/FT blends are studied and compared with JP-8. Experiments included in this research involve studying the combustion instability patterns, mapping emission levels and determining the sooting proclivity of the alternative fuels and blends. Results of this study indicate that the FT fuel produces lower soot volume fraction and emissions; however, this fuel cannot be used solely in current combustors due to inadequate seal swelling characteristics and fuel lubricity requirements. JP-900 and (25/75), (50/50) JP-8/FT blends, on the other hand, show acceptable results and, hence, can directly replace the existing JP-8 fuel, thereby reducing the dependence on crude imports.

Table of Contents

List of Figures

List of Tables

Nomenclature

Abbreviations

CA	cooling air
EIA	Energy information administration
FN	flow number
HDT	hydro treated
L	path length
LCO	light cycle oil
MW	molecular weight
NP	nitrogen purge
OD	outside diameter
PAH	poly aromatic hydrocarbon
PM	particulate matter
PPM	parts per million
PT	pressure transducer
RCO	refined cycle oil
TC	thermocouple

Symbols

ϕ	equivalence ratio
φ	swirl vane angle of air swirler
λ	wavelength
c	chord length of air swirler
D_H	hub diameter of air swirler
D_N	exit diameter of nozzle
f_v	soot volume fraction
k_{ext}	extinction coefficient
m	refractive index of soot
N	moles
S_N	swirl number
T_{up}	temperature upstream of combustor prior to inlet venturi
X_i	mole fraction of species i

Acknowledgements

I am most grateful and indebted to my thesis advisor, Dr. Robert Santoro for giving me an opportunity to work under him and kindly providing guidance throughout the development of this study. He has been the source of inspiration and his support, encouragement, patience and his comments have been of greatest help at all times. I would like to sincerely thank Dr. Seong-Young Lee and Dr. Chirstopher Mordaunt for helping me immensely with this research, teaching me the basics of experimental combustion, chemically reacting flows and getting me acquainted with the high-pressure system instrumentation. I would also like to thank Dr. Thomas Litzinger for his invaluable suggestions during weekly meetings and for reviewing my thesis.

I would like to express my gratitude towards my fellow colleague Amy Mensch, who helped me with these experiments, her timely inputs and suggestions have helped me enormously throughout the duration of this research. Additionally, I extend thanks to Arvind Menon and Venkatesh Iyer for their invaluable contributions and suggestions. I am grateful to Mr. Larry Horner and Mr. Larry Schaff for their troubleshooting solutions to all the instrumentation and fabrication related problems and Mrs. Ginny Smith and Mrs. Mary Newby for their exemplary administrative assistance. Finally, I want to thank Dr. Ron Wasco for helping me with the H/C ratio measurements and Dr. Dania Fonseca for obtaining the GC-MS analyses.

I take this opportunity to express my love and sincere thanks to my parents for their endless love and support. They taught me the value of hard work and provided me with enormous support throughout my life.

Chapter 1

Introduction

The aviation industry has been dependent solely on gas turbine engines for providing the driving thrust for many years. It is evident that the gas turbine engines provide high efficiencies and robustness with the requirement of low maintenance costs. These aviation gas turbine engines currently use petroleum-based jet fuels such as JP-8 and Jet-A. However, fluctuating costs and availability of these fuels is a major concern. Coal-based fuels can replace existing jet fuels, provided that these fuels meet the current emission standards and exhibit physical and chemical properties, which can be compared to existing jet fuels, in order to use them in current combustors without altering the present turbine engine geometry.

This following section will establish a platform for the current research work by discussing various factors that affect combustion in gas turbines like emissions, mean soot volume fractions and combustion instability. This is followed by a description of the motivation for the current research and objectives.

1.1 Soot Production Mechanisms

The formation of soot particles in combustion systems fundamentally involves four processes: soot precursor formation; particle inception; surface growth and soot oxidation. From a fuels perspective the soot precursor formation is of the most interest as

fuel composition can drastically affect the propensity to form soot. Precursor chemistry can be viewed as the growth of small hydrocarbon species such as C_2H_2, C_2H_3, C_3H_3, etc that lead to the formation of the first aromatic ring. The importance of aromatic ring formation is based on studies of soot particles extracted from combustion systems that have shown a disordered structure that requires the formation of poly aromatic hydrocarbons.

Frenklach *et al.* [1, 2] showed that for fuels with larger aliphatic content soot formation is dependent on formation of first aromatic ring. Formation of this first ring is a rate limiting step for soot production in case of aliphatics. Once the aromatic ring is formed, it reacts with a non-aromatic species for e.g., acetylene, initiating a reaction sequence which further leads to formation and growth of PAHs (see Figure 1-1). The mechanism leading to the formation of aromatic species is given by Frenklach is shown in Figure 1-1.

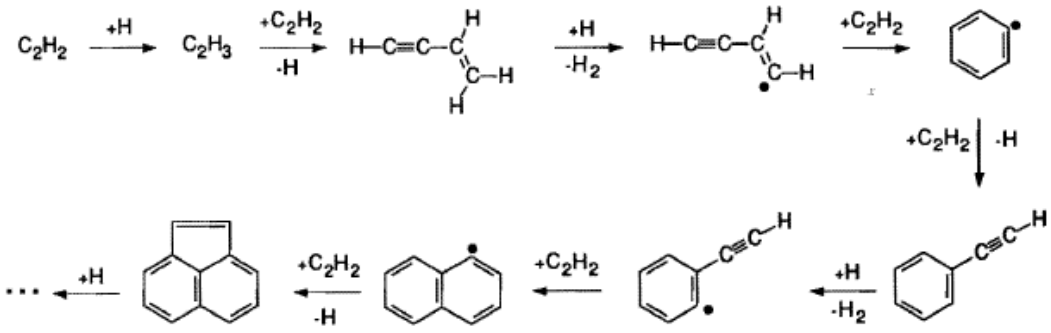

Figure 1-1 Simplified soot formation mechanism (source: [2])

This mechanism for soot formation is commonly known as the Hydrogen-Abstraction-Acetylene-Addition (HACA) mechanism. Figure 1-1 shows the process of soot formation starting from an acetylene molecule but extensions to other hydrocarbon species have been developed. Initially hydrogen addition occurs to form C_2H_3, which is subsequently followed by addition of acetylene to form butadienyl (n-C_4H_5•). Further, hydrogen abstraction and acetylene addition gives rise to a phenyl radical (c-C_6H_5•) that is cyclic in nature. Recent studies have also showed that another important pathway for soot formation exists that involves chain initiation by C_3H_3 molecules, which is generally added to soot formation mechanisms. The process of hydrogen abstraction and acetylene addition subsequent to phenyl radical formation produces multiple ringed structures thus resulting in formation of stable chemical species (like acenaphthylene).

The above discussion focuses on the aliphatic fuel. For aromatic compounds the formation of the first aromatic radical is achieved by hydrogen abstraction from the aromatic ring. Thus, aromatic species by pass the $C_2 - C_4$ mechanism described above. As a result the presence of aromatic components in fuels provides a fast chemical route to soot formation.

As will be discussed later, JP-8 shows higher amounts of aromatic content and based on above mechanism JP-8 is expected to show higher sooting tendency. On the contrary, FT fuel shows higher aliphatic content and JP-900 shows greater concentration of saturated hydrocarbons. These fuels are expected to produce less amounts of soot compared to JP-8.

1.2 Emissions: Production Mechanisms and Reduction Strategies

1.2.1 NO_x Formation Mechanisms

In general our current understanding of NO_x formation for hydrocarbon fuels involves three mechanisms: Zeldovich mechanism (thermal); Fenimore (prompt) mechanism and N_2O-intermediate mechanism [3].

1.2.1.1 Zeldovich Mechanism

This mechanism is a set of three reactions.

$$O + N_2 \Leftrightarrow NO + N \quad \textbf{1.1}$$

$$N + O_2 \Leftrightarrow NO + O \quad \textbf{1.2}$$

This is extended by a third reaction as follows

$$N + OH \Leftrightarrow NO + H \quad \textbf{1.3}$$

Reaction 1.1 has strong temperature dependence and, consequently, as a thumb rule this mechanism is important at temperatures above 1800 K. NO formed following this mechanism is a slower process as compared to combustion time scales and it is usually observed in post-combustion processes. However, super equilibrium concentrations of O and OH radicals can occur within the flame zone, which results in an increase in NO formation rate. For lean premixed pre-vaporized conditions temperatures below 1800 K are typically achieved. For these conditions the Zeldovich mechanism is not important in

the prediction of NO_x. However, mechanisms discussed next are important at lower temperatures.

1.2.1.2 Fenimore Mechanism

Fenimore found that some NO is produced very quickly in the flame zone of laminar premixed flames. This process is faster as compared to the thermal NO production. In this mechanism, hydrocarbon radicals form amines or cyano compounds in presence of nitrogen from the combustion air and further react to form NO [3].

$$CH + N_2 \Leftrightarrow HCN + N \quad \textbf{1.4}$$

$$C + N_2 \Leftrightarrow CN + N \quad \textbf{1.5}$$

$$HCN + O \Leftrightarrow NCO + H \quad \textbf{1.6}$$

$$NCO + H \Leftrightarrow NH + CO \quad \textbf{1.7}$$

$$NH + H \Leftrightarrow N + H_2 \quad \textbf{1.8}$$

$$N + OH \Leftrightarrow NO + H \quad \textbf{1.9}$$

These reactions have lower activation energies thus allowing NO to form at lower flame temperatures. Generally, this mechanism is effective at equivalence ratios below 1.2. Figure 1-2 shows a schematic layout of the different reaction pathways for Fenimore mechanism.

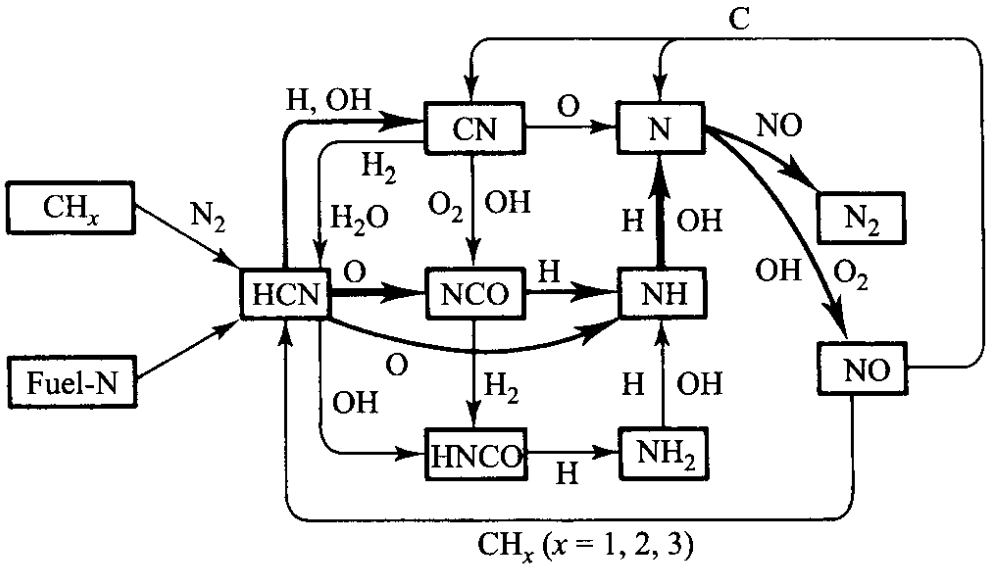

Figure 1-2 NO formation by the Fenimore mechanism (source: [3])

1.2.1.3 N_2O-Intermediate Mechanism

The N_2O mechanism is a set of three reactions as follows

$$O + N_2 + M \Leftrightarrow N_2O + M \quad \textbf{1.10}$$

$$H + N_2O \Leftrightarrow NO + NH \quad \textbf{1.11}$$

$$O + N_2O \Leftrightarrow NO + NO \quad \textbf{1.12}$$

It is important at lower temperatures and lean combustor operating conditions ($\phi < 0.8$) and so this mechanism is significant for gas turbines, especially those which employ lean-premixed prevaporized (LPP) combustion.

1.2.2 NO_x Control Strategies

This section describes methods that are found effective in controlling NO_x emissions in gas turbines. Water injection technique is explained first. Rich-quench-lean method is explained next subsequently followed by selective catalytic reduction method.

1.2.2.1 Water Injection Technique

Water injection techniques are among the oldest techniques used for lowering the combustion products temperature. Using direct injection of water into the combustion zone reduces the overall temperature and subsequently the amount of NO_x produced. This method has certain drawbacks that include: an increase in CO and unburned hydrocarbon (UHC) emissions as combustion deteriorates with water injection [4]; an increase in fuel consumption, which is required to heat up the water to combustion temperature; and finally, an increase in the maintenance cost of the components situated downstream of the combustor due to presence of water in combustion products. Additionally, injection of water in the combustion zone will require additional water storage, purification facilities and supply systems that would increase the capital and the operational costs.

1.2.2.2 Rich-Quench-Lean Technique

Rich-Quench-Lean, or staged combustion method, uses the fact that the combustion temperature is significantly lower at very rich and very lean equivalence ratios. In this technique, the combustion process is initiated at stable fuel-rich conditions

resulting in lower NO_x formation and the products of combustion are rapidly mixed with additional air such that the overall equivalence ratio drops down to the fuel-lean region. The temperature in the lean-burn zone must be controlled to an optimum value such that it is neither so high to promote NO_x formation nor so low as to prevent the consumption of CO, UHC and soot.

1.2.2.3 Selective Catalytic Reduction

Selective catalytic reduction methods are also used to eliminate NO_x. In this technique, a catalyst is used in conjunction with ammonia to reduce NO in the combustion products to N_2. This method is effective for temperatures ranging from 400^0F to 950^0F. Such combustors can operate at lower overall temperatures and equivalence ratios. However, there are several drawbacks like cold start, catalyst activation at lower temperatures, high initial and operating costs. This method is best suited for natural gas fired turbines.

1.2.3 Carbon Monoxide Formation and Reduction Strategies

Carbon monoxide forms as a result of incomplete combustion. This generally occurs in combustors, which run fuel-rich or have low residence time. However, CO formation at lean conditions is also possible and is caused by one or more of the following [4]:

1. Incomplete combustion caused by fuel/air ratios that are too low and/or insufficient residence times.

2. Insufficient mixing of fuel air causing regions to have local equivalence ratios that are either very lean or very rich causing incomplete combustion resulting in high concentrations of CO locally.

3. Quenching of the hot combustion products by combustor cooling air that is entrained downstream of the combustion zone can yield CO.

Often factors that influence CO emissions include combustor inlet temperatures, combustion pressure and spray atomization in case of liquid fueled turbines.

The following methods are effective in CO emission reduction [4].

1. Maintaining an overall equivalence ratio of $\phi = 0.8$ in the primary combustion zone, which is an optimal value for lowest CO production.

2. Increasing residence time to ensure complete combustion.

3. Higher liner wall temperature by reduction in liner wall cooling air.

4. Reduction in drop size by improved atomization process [5].

1.3 Combustion Instability

Combustion instability is one of the concerning factors for gas turbine operation. It can result in severe damage to the combustor components. Combustion instability is characterized by large amplitude, unsteady pressure oscillations in the combustion chamber pressure occurring at frequencies characteristic of the acoustic modes of the combustor, especially in turbines, which employ lean combustor operation. Although, combustion instability is dependent on the combustor geometry, other factors like injection pattern, air flow rates, fuel-air mixing rates, inlet temperatures, and amount of

swirl also affect it. It is difficult to determine the exact mechanisms that are responsible for combustion instability. Usually, instabilities are initiated by small perturbations that result in coupling between the heat release and pressure fluctuations. The pressure oscillations grow to a value where the energy supplied cannot be overcome by the energy losses in the system and a limit cycle is reached [6]. Gas turbine combustors may show a different stability map corresponding to different fuels, hence it is necessary to test newer fuels and compare their stability maps with reference fuels, like JP-8 in the current study.

Mongia and his colleagues at GE aircraft engines [7] have studied causes and control strategies of combustion instability mechanisms exhibited in some of their recent combustors. Three types of coupling mechanisms are explained for the occurrence of combustion instability. The first class of coupling essentially arises from interaction between the pressure disturbances and flame position and shape details. The second class represents coupling between the local equivalence ratio and pressure oscillations. This often occurs as a result of slight changes in the fuel and the air flow rates locally, as well as changes in the spray characteristics of the injectors. The third class is related to the coupling that arises out of intermittent blowout. This happens at very lean conditions and is a very low-frequency phenomenon (< 500 Hz). Figure 1-3 presents a schematic of the components in a gas turbine and their inter-relation acoustically. Such models are used to link the acoustic characteristics of the individual components with each other. Ducruix *et al.* [8] have provided a sound mathematical background on modeling different coupling mechanisms, which relate heat release fluctuations and the pressure fields in gas turbine combustors. However, designing stable combustors still involves previous empirical

relationships that work for specific well known combustor geometries. New designs that deviate from these geometries will likely experience combustion instabilities at some point in their development program.

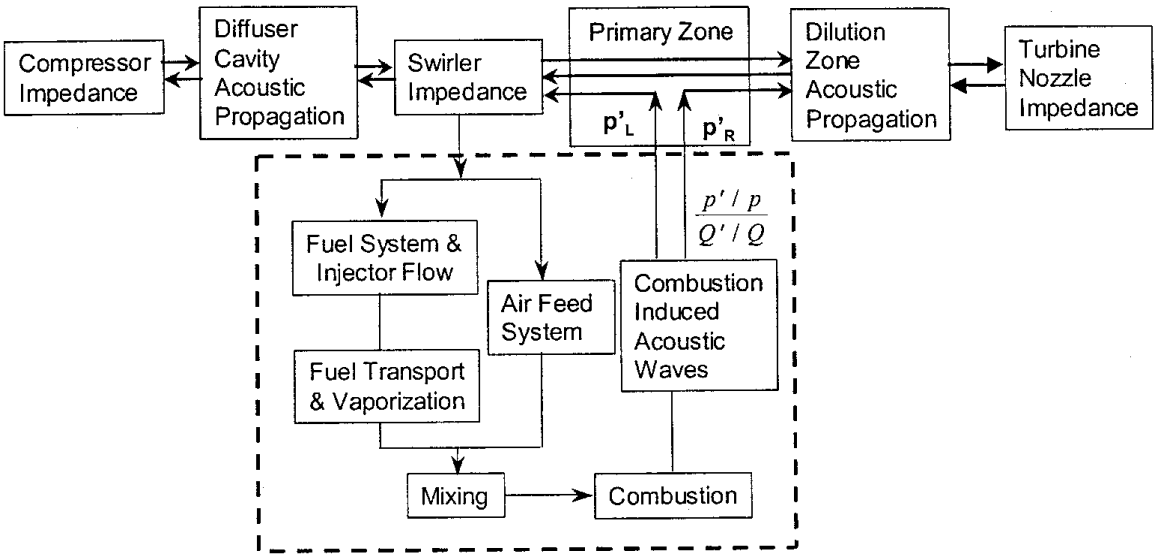

Figure 1-3 Framework for combustor dynamics modeling (source: [7])

1.4 Motivation for Current Work

Modern-day aviation gas turbine engines demand higher temperatures and pressures to achieve better performance and power. This has given rise to many new technical challenges with regards to the cooling of the combustor linings as well as development of better materials for the components downstream of the combustion chamber, which could sustain higher operating pressures and temperatures. One of the possible solutions suggested is to use a fuel that can serve as coolant for varying combustion conditions [9]. However, this fuel is also expected to meet all the combustion requirements, like higher combustion efficiency, lower emissions and good combustion

stability, without making any changes to the current combustion chambers. The increasing need to reduce the pollutant emissions and dependence on foreign fuels are equally compelling reasons to propel research for alternative fuel sources.

The following discussion deals with the statistics of U.S. fuel consumption, which will further make clear the aspect of requirement of alternative fuels.

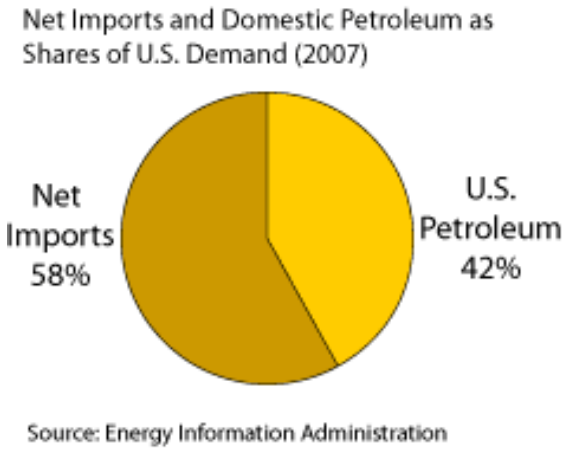

Figure 1-4 Net Imports v/s Domestic production of crude oils (Source: EIA)

Imports of crude oil in 2007 as reported by EIA (Figure 1-4) were 58% of total U.S. crude oil requirements. It can be observed that the U.S. fuel consumption has steadily increased over years but, production of crude oil within U.S. has not matched the growth in the consumption (Figure 1-5) and as a result of which, the U.S. has become more dependent on international sources for its crude oil supplies. This has led to a search for alternate sources of fuels, especially those that can be obtained from nationally owned sources.

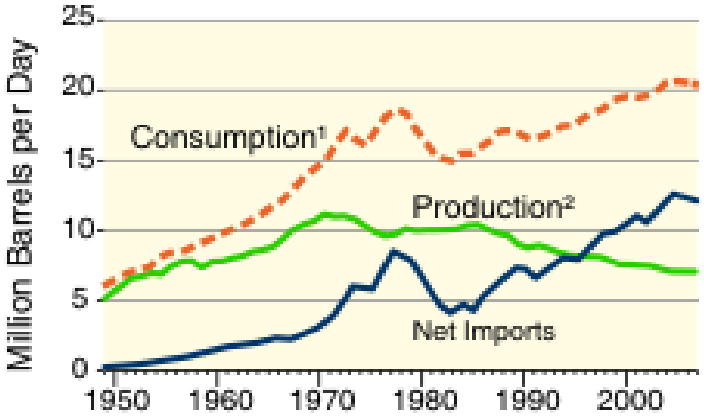

Figure 1-5 Production of crude oil within U.S. v/s consumption and imports (Source: EIA)

1.5 Description of the Jet Fuels Studied

Three fuels and their blends are compared in the current study and the fuels are: JP-900, JP-8 and Fischer-Tropsch (FT).

The current study includes JP-8 fuel, which is widely used by the U.S. Air Force and military for defense related aviation and ground applications. This fuel is an improved adaptation of commercially available Jet A/Jet A-1 jet fuels. Its properties are enhanced by three additives, as specified by the military: a corrosion inhibitor/lubricity improver; fuel system icing inhibitor; and anti-static additive. Edwards *et al.* [10, 11] have presented the physical and chemical properties of JP-8. Further, JP-8+100 is a program introduced to improve the thermal stability of this fuel by adding certain class of additives [11, 12]. This program aimed at improving the thermal stability of JP-8 from 325^0F to 425^0F. However, JP-900 fuel under current study has capabilities to meet even higher demands of heat loads and can be stressed to temperatures in the vicinity of 900^0F and is discussed next.

JP-900 is a coal-derived fuel obtained from PARC Technical Services, Harmarville, PA. This fuel is produced by direct liquefaction of coal feedstock. Burgess and Schobert [13] showed that two-ringed compounds can be obtained from direct liquefaction of coal with a dispersed, sulfide molybdenum catalyst followed by the caustic washing to remove the by-product phenols. Further, hydro treatment of this mixture and addition of certain additives gives rise to a blend, which exhibits excellent thermal stability. Following this work, Blaster *et al.* [14] further presented a detailed analysis of the development of JP-900 fuel. The initial developmental JP-900 samples essentially contained 1:1 mixture of coal-derived refined chemical oil (RCO) and petroleum-derived light cycle oil (LCO). This mixture has demonstrated excellent heat sink capabilities and agreement with most of the characteristics of JP-8 [14]. Furthermore, a detailed comparative study between hydro-treated (HDT) RCO/LCO 1:1 (X-610), HDT RCO/LCO 3:1 (X-620) and JP-8 fuels is presented by Lee *et al.* [15], which provides information with respect to the soot volume fractions, NO_x and CO emissions of these early developmental JP-900 samples compared with JP-8.

The quest for alternative fuels has also led to a research that includes fuels that are being developed using the Fischer-Tropsch (FT) Process [16, 17]. FT is an alternative fuel, which is usually produced by partial oxidation of coal or natural gas in presence of steam and oxygen and a catalyst to produce carbon monoxide and hydrogen (syngas). Fischer-Tropsch reaction converts this syngas into paraffinic hydrocarbons, which are eventually refined to the desired products [16]. A schematic of this process is presented in Figure 1-6 [18]. FT fuels obtained by this process are highly paraffinic in nature with

very little or no aromatic content. This fuel is expected to exhibit low sooting and emission characteristics. However, aromatic content is believed to be essential for sufficient swelling of O-rings, bladders and other seals within the fuel delivery and circulation systems. Graham *et al.* [19] have discussed the effects of blending different aromatics with FT fuel on the amount of swell induced on nitrile rings. A different approach is to improve FT fuels swelling capability by introducing certain additives. Dirk *et al.* [20] and Dewitt *et al.* [21] have shown that species such as phenols, naphthols, and benzyl alcohol (which primarily have aromatic content) are all promising additives. However, considering the environmental concerns and fuel performance, benzyl alcohol is a better choice. It is also demonstrated that a 50/50% by volume mixture of Jet A-1 and FT fuel does exhibit properties that fall within the permissible range specified for jet fuels [17, 22, 23] but, blending FT fuel with aromatics results in increased particulate matter (PM) emissions, which is a result of increase in concentration of aromatic compounds responsible for PAH formation. The current study includes blending FT with JP-8 and compares emission characteristics, soot volume fractions with individual fuels. The FT fuel under study (also known as S-8 Synthetic Jet fuel) is supplied by Syntroleum Corporation, Tulsa, Oklahoma.

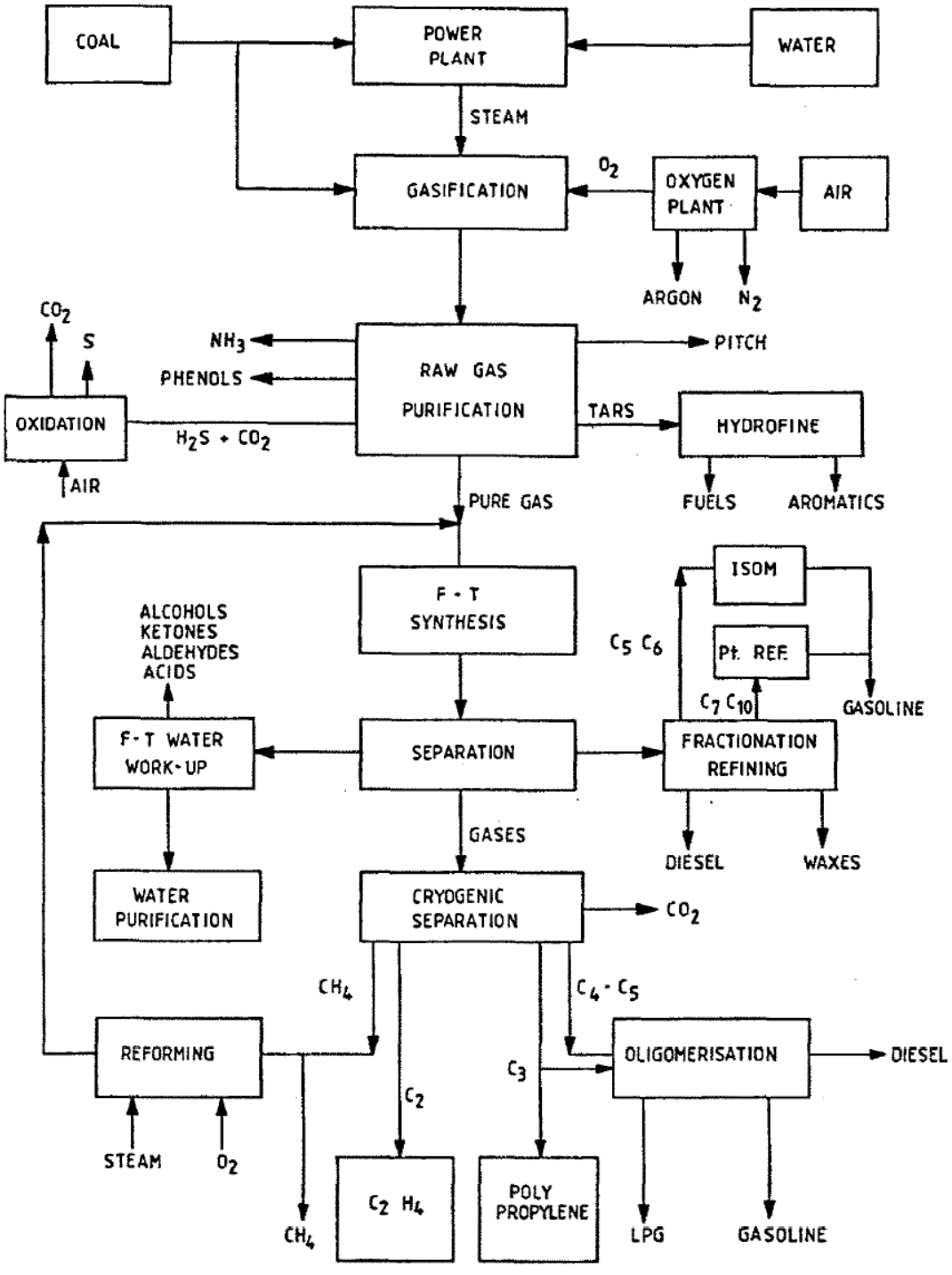

Figure 1-6 Schematic of Fischer-Tropsch process (Source: [18])

Chapter 2

Experimental Apparatus and Techniques

2.1 Air Delivery and Metering System

The air delivery setup consists of an American Air (Type ES2) compressor that delivers air at a maximum flow rate of approximately 50 g/s and at a pressure of 2.42 MPa. This air is metered with the use of 4 critical venturi orifices with throat diameters of 2.84, 3.81, 4.95, and 7.39 mm, respectively. Either individual or combinations of two or more orifices can be used to obtain the desired air flow rates. In order to obtain correct air flow rates, the temperature and the pressure, upstream of these critical venturi orifices are measured through the use of static pressure transducer (PT) and thermocouple (TC) as shown in Figure 2-1. This setup also includes a jewel orifice (1.14 mm) used to meter the cooling air, which is subsequently used to prevent the liquid fuel from vaporizing prior to injection in the combustor. A more detailed description of the liquid fuel cooling is provided in section 2.3.4. A schematic of the air supply and metering system is shown in Figure 2-1.

2.2 Gaseous and Liquid Fuel Delivery Systems

The model gas turbine combustor is made to support gaseous as well as liquid fuel combustion. The gaseous fuel delivery system is used in current experiments to establish an initial flame from which a transition to liquid fuel operation is achieved. The liquid

fuel delivery system is used to vary the liquid fuel flow rate as required in the combustor. The following sections describe these two systems in detail.

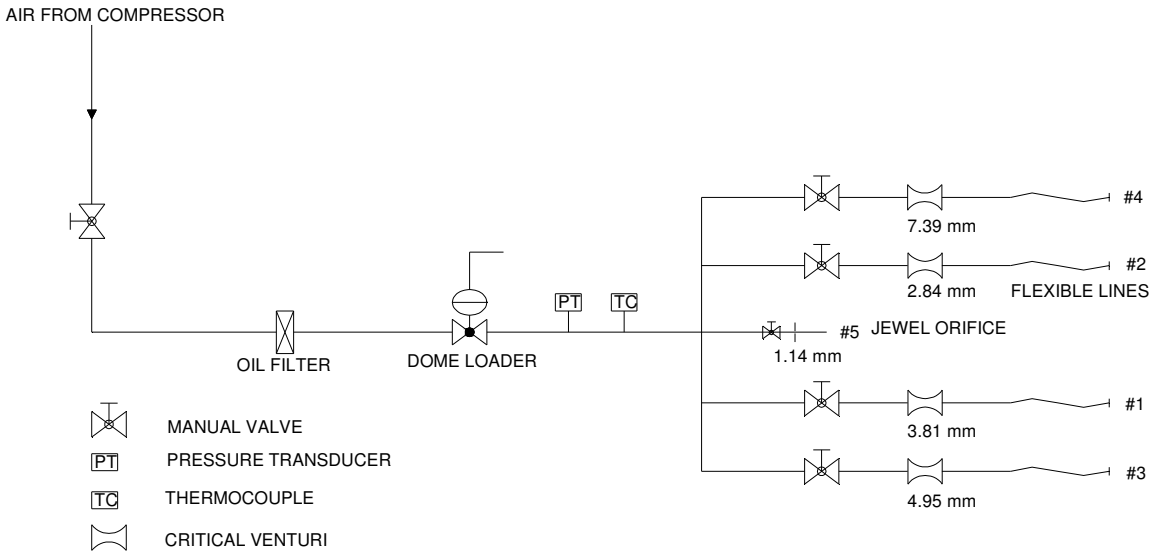

Figure 2-1 Schematic of compressed air delivery system

2.2.1 Gaseous Fuel Delivery System

Compressed natural gas (CNG) is used as gaseous fuel in the present study. The low-pressure commercial gas is pressurized to about 13.79 MPa using a Fuelmaker Vehicle Refueling Appliance (Model FM4) and is stored in an array of 7 cylinders in an external fuel shed.

The gaseous fuel delivery system is controlled by a set of pneumatic and dome loader valves and fuel is metered using a jewel orifice of 0.762 mm diameter. In addition, provisions are made for purging the fuel lines with nitrogen at the beginning and end of

the experiment and all the pneumatic valves are configured to provide quick fuel shut off and activation of the nitrogen purge in the event of an emergency. A schematic of the gaseous fuel delivery and metering system is shown in Figure 2-2.

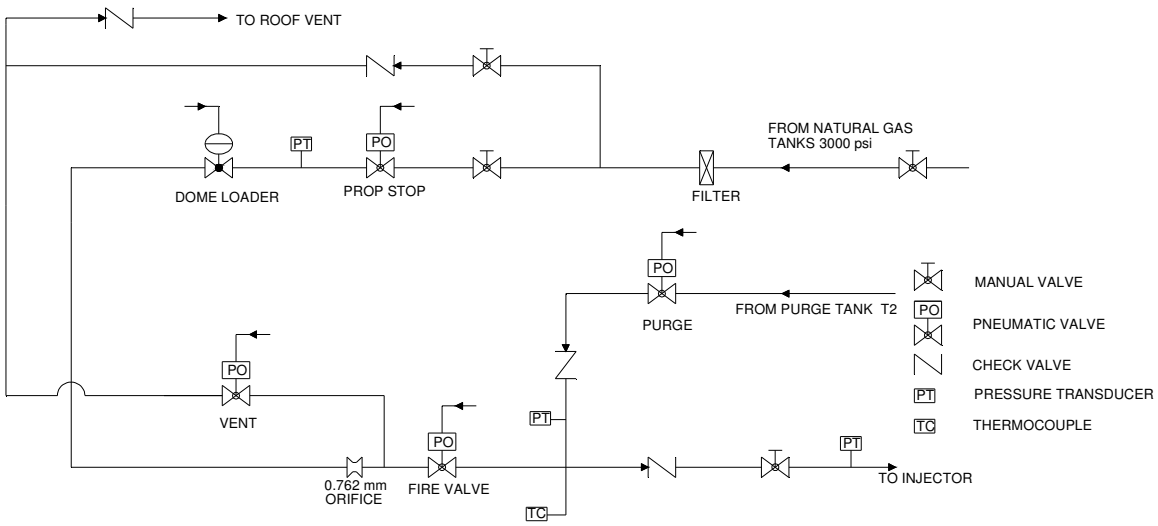

Figure 2-2 Schematic of gaseous fuel delivery and metering system

2.2.2 Liquid Fuel Delivery System

Figure 2-3 shows a schematic layout of the liquid fuel delivery and metering system. In this system, liquid fuel is stored in three tanks situated in the external fuel shed, which have approximate capacity of 48 Liters. The liquid fuel tanks are pressurized using helium to an approximate pressure of 3.5 MPa and the fuel flow is metered using an electronically controlled, variable area, cavitating, needle valve (Whitey, Model SS 21RS4) and a Hoffer turbine flow meter (model MF 1/2x30B). In addition, a trickle purge is provided as shown in figure. This is used to maintain a minimum pressure in the

fuel line, which helps in preventing the combustion products or air from entering the injector tube, especially during transitioning from gaseous to liquid fuel and liquid fuel shut-off. In such cases the pressure inside the injector tube is low as compared to the combustor pressure and there exists a possibility of combustion products getting into the injector tube as well as blocking the liquid fuel injector.

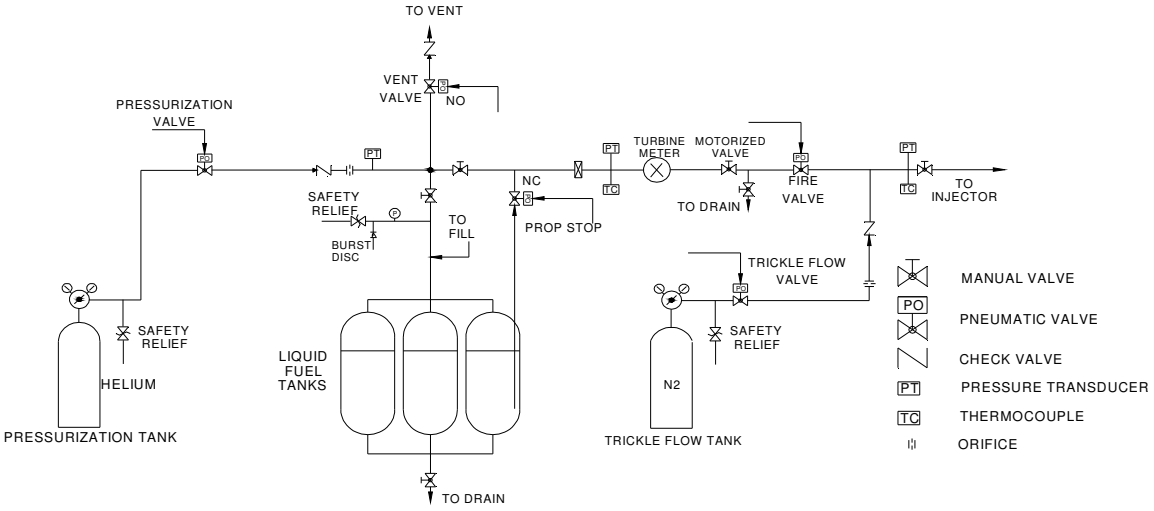

Figure 2-3 Schematic of liquid fuel metering and delivery system

2.3 The Model Gas Turbine Combustor

2.3.1 The Combustor Setup

Figure 2-4 shows the schematic of the model gas turbine combustor setup. This combustor is designed to run at high pressures (up to 2 MPa) and high inlet temperatures (up to 800K). Regenerative or non regenerative cooling approaches can be used to cool the combustor walls. The regenerative method is used for the experiments and is discussed next. As shown in the figure, compressed air enters the outer section of the chamber after being metered. This air is used to cool the combustion chamber walls and to remove heat from the exhaust section. It is then passed through an electric heater (Watlow process systems Model 700, 140 kW), which is capable of heating air to 800 K at a maximum flow rate of 50 g/s. This heated air flows through a choked inlet venturi of 7.39 mm diameter and enters the injection portion of the apparatus. The air then passes through a swirler, discussed later in section 2.3.3. A mixture of air and fuel enter through the dump plane of the modular combustor where this mixture is ignited. The combustion products then exit the combustor through a choked exit nozzle with a diameter of 10.16 mm, from where they pass into the exhaust section. The inlet choked venturi and the exit choked nozzle acoustically isolate the combustion chamber from the air inlet and the exhaust stack. This arrangement provides a steady mass flow rate upstream of the inlet venturi in spite of any pressure oscillations by combustion instabilities within the combustion chamber. Pressure fluctuations in the exhaust stream are also blocked by the exit nozzle from travelling into the combustion chamber.

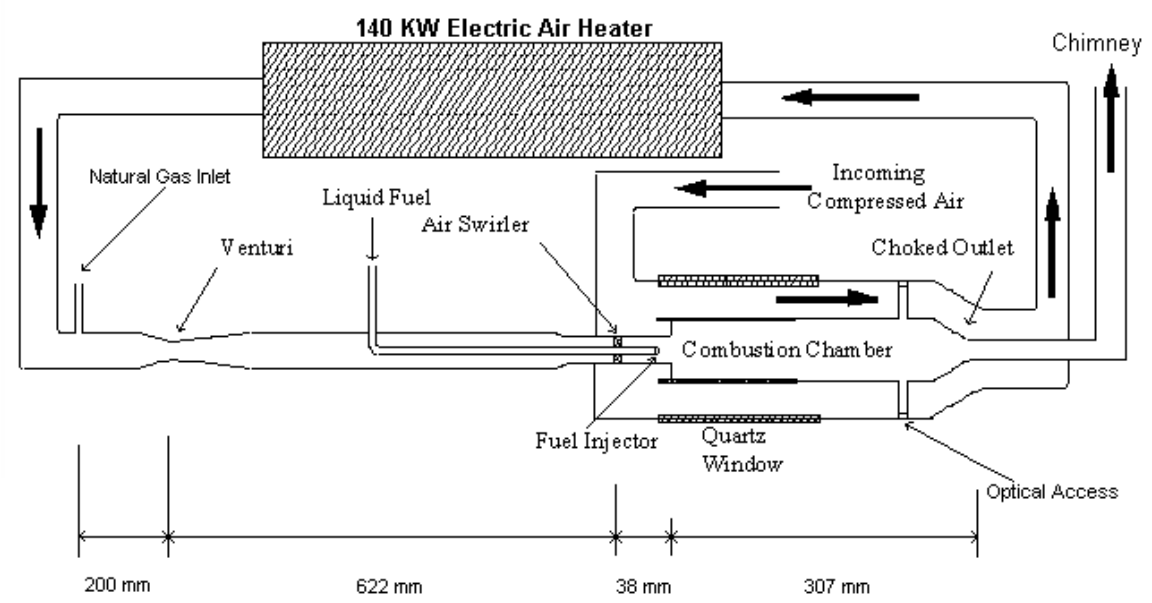

Figure 2-4 Schematic of the model gas turbine combustor (not to scale)

This system can be operated with either natural gas or liquid fuels. For the case of natural gas, the fuel is introduced in the chamber upstream of critical venturi as shown in Figure 2-4. In the case of liquid fuels, to achieve a stable flame, natural gas is ignited first, and then liquid fuel is introduced in the system as discussed earlier. The flow rate of natural gas is reduced and that of the liquid fuel is increased until a stable flame is achieved. The natural gas is eventually cut off for liquid fuel experiments.

Figure 2-5 shows the gas turbine monitor and control system, which is used to monitor critical parameters of the model combustor. It comprises of a series of pressure transducers (Setra) to measure static pressures (PT) and K – type thermocouples to monitor the temperatures (TC). A separate pressure transducer (DPT) is used to measure differential pressure across the quartz section in the combustion chamber. In this figure is

also shown, the nitrogen purge system that is used to purge the combustion chamber in case of an emergency or flame blowout. Additionally, this figure shows the nozzle cooling system. A constant flow rate of air (2.7 g/s) obtained by metering the building air using an orifice plate and variable flow rate of water is used to achieve nozzle cooling. The air is used to atomize the nozzle water for effective cooling. The exhaust temperature of exit nozzle is maintained at approximately 450 K by controlling the amount of cooling water using Masoneilan valve (MV), which utilizes a variable throat area to control the flow rate of water. The actuation of these valves is achieved using the building air supply.

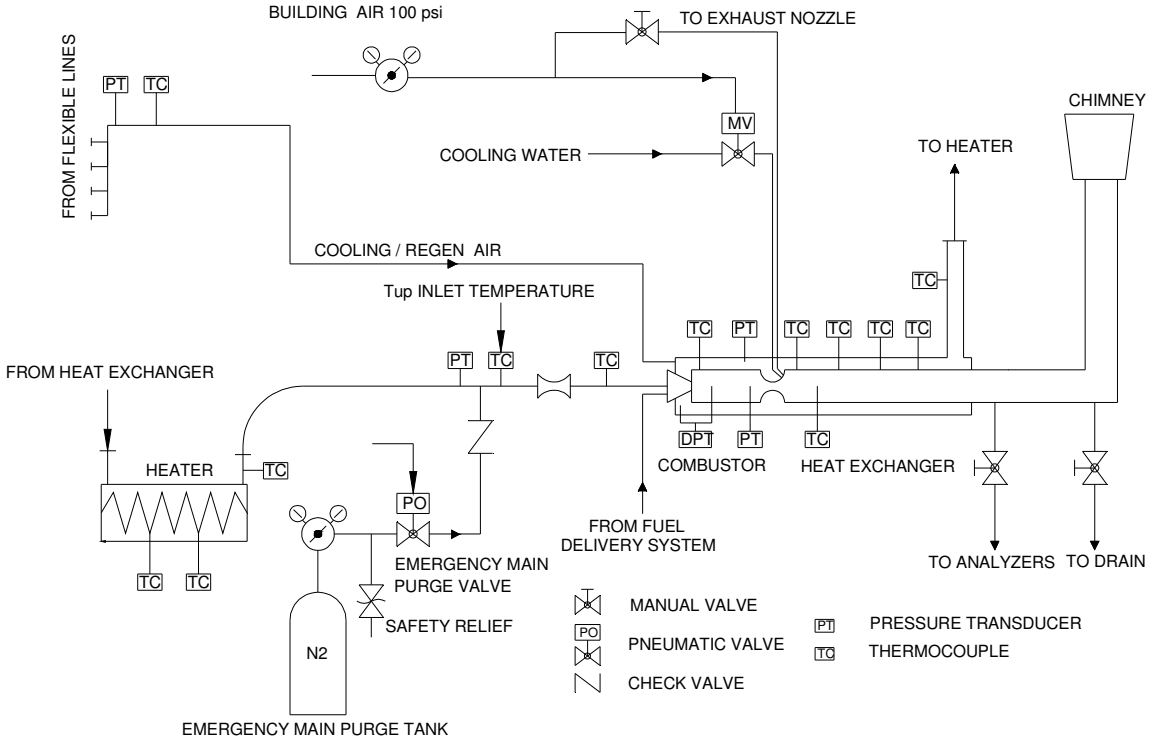

Figure 2-5 Gas turbine monitor and control system

2.3.2 The Combustion Chamber

The model gas turbine combustor has a modular design with optical access to the chamber. This modularity allows the flexibility to vary the chamber length. A sectional view of the chamber configuration, which is used for the current experiments is shown in Figure 2-6 and explained next. The outer section has provisions for passage of cooling air, which helps in removing the heat from the combustion chamber. This air is preheated further to a known inlet temperature by the heater. This preheated air, after passing through swirler, mixes with the liquid fuel in the annular region between the 9.53 mm diameter injector tube and 20 mm diameter inlet tube. This fuel air mixture is then introduced in the 45 mm diameter 307 mm long cylindrical modular combustion chamber. The quartz chamber, which is 2mm thick and 114 mm long, provides optical access to the chamber. The cooling passage is designed to force air on the quartz window to avoid overheating, while also maintaining a small pressure differential across the chamber. This air also impinges on the 19 mm thick windows in the exterior section. The optical section of the chamber is succeeded by two stainless steel sections, 114mm and 51 mm respectively. These sections are coated with zirconium oxide to prevent overheating and are mounted with water-cooled pressure transducers (PCB) for high frequency pressure measurement. Additionally, the 51 mm section is mounted with two quartz windows in order to facilitate laser extinction measurements, which is discussed in detail in section 2.4. The last section of the combustion chamber is a 10.16 mm diameter, 30^{o} exit nozzle. This nozzle section is water-cooled externally. As discussed earlier, air is injected along with the nozzle water to provide better atomization at the exit

of the nozzle. This atomized water helps to cool the combustion products as they enter the exhaust section.

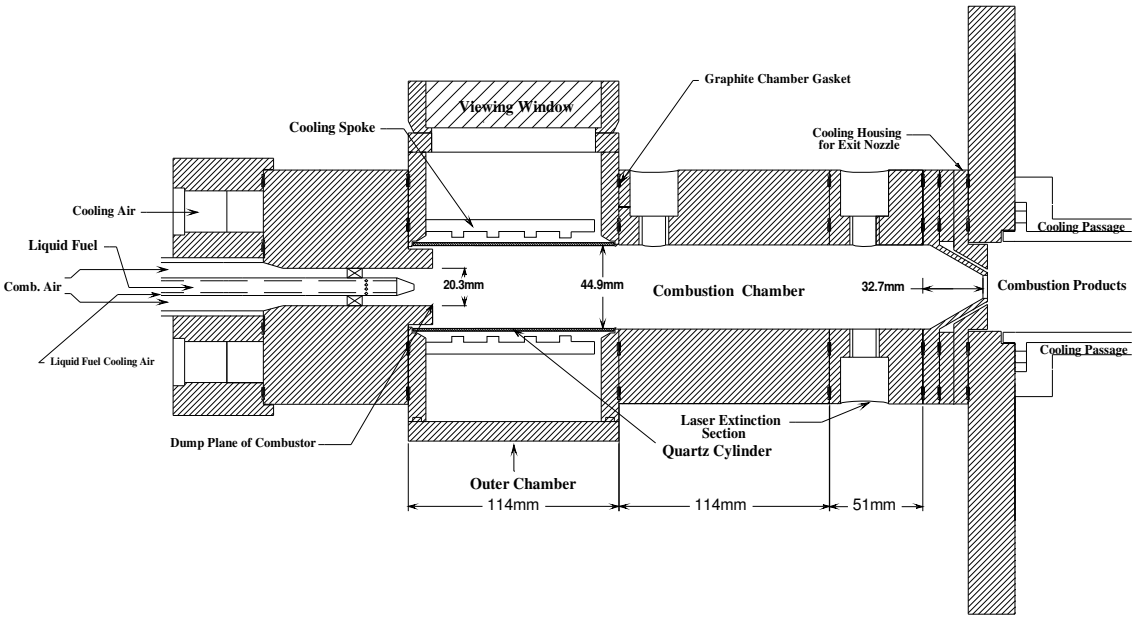

Figure 2-6 Sectional view of the combustion chamber

All the sections discussed above have grooves for two graphite gaskets, which prevent leakages between the inner and the outer sections as well as leakages outside the chamber. These sections are aligned using pins and a hydraulic jack is used to force all the components of the combustion chamber together against the exhaust heat exchanger. The exhaust heat exchanger comprises of two concentric tubes. The inner tube carries the combustion products along with the atomized nozzle water injected at the nozzle exit, whereas the outer tube carries the cooling air.

2.3.3 Inlet Air Swirler

To ensure proper mixing of air and liquid fuel, swirl is introduced in the inlet air 38 mm upstream of the dump plane. Swirler helps in stabilizing as well as anchoring the flame. The air swirler used in the current study is shown in the Figure 2-7.

Swirl strength of a swirler is an important parameter in selection of a swirler and it can be characterized using the swirl number, S_n [24], which depends upon the geometry of the swirler. This swirl number can be calculated using Equation 2.1, which assumes the vanes to be very thin and having a constant chord length, c, where φ is the vane angle, and D_h and D_n are the hub diameter and nozzle tube diameter respectively [4, 24]. In the current study, a 45^o swirler is used for all the experiments. The S_n for this swirler, calculated using Equation 2.1, is approximately 0.69, assuming uniform axial and swirl velocities.

$$S_n = \frac{2}{3}\left[\frac{1-(D_h/D_n)^3}{1-(D_h/D_n)^2}\right]\tan\varphi \qquad \textbf{2.1}$$

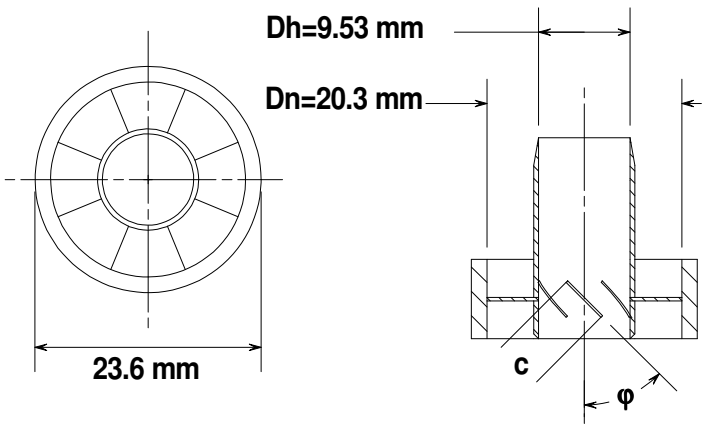

Figure 2-7 Schematic diagram of swirler, vane angle = 45^0

2.3.4 Liquid Fuel Injector

The liquid fuel injector setup consists of two concentric tubes. The outer tube carries air and the inner tube carries liquid fuel. A Delavan pressure atomizer (also commonly known as a peanut injector), which is secured at the end of the injector tube, is used to inject a hollow spray of fine liquid droplets in the combustion chamber. The differential pressure across this injector enables it to produce a fine spray of liquid fuel at a high velocity into the combustion chamber. The injector used in the current experiments is a Delavan # 27700-5 that produces a 85^0 hollow cone angle at a flow number (FN_{US}) of 1.9 shown in Figure 2-8. The outer tube, which carries cooling air as stated earlier, is used to prevent the liquid fuel in the inner tube from vaporizing before reaching the fuel injector, which is undesirable as two phase flow considerably increases the pressure drop across the injector. This cooling air is injected into the combustion chamber perpendicular to main air flow just upstream of the injector through 10 equispaced 0.762 mm diameter holes. Due to the design of the injector section, the Delavan nozzle is exposed to the flame, which is quite close to the nozzle. This result in overheating and possible coke formation that causes some concern regarding the uncertainty and reproducibility of the results reported.

Flow area of a pressure atomizer, which is an important parameter in its selection, can be effectively measured by defining the flow number [25]. Equation 2.2 presents the flow number in the form for English units and this form assumes a constant fluid density, which is 765 kg/m^3, since this density represents the general category of aviation jet

fuels. Equation 2.3 presents the flow number in S.I. units. Equation 2.4 provides relationship for converting the values in English units to S.I units.

Figure 2-8 Delavan pressure atomizer # 27700-5 FN_{US} 1.9 spray angle 85^0

$$FN_{US} = \frac{\text{Flow rate (lb/hr)}}{(\text{Injection pressure differential, (psid)})^{0.5}} \qquad \textbf{2. 2}$$

$$FN_{SI} = \frac{\text{Flow rate, (kg/s)}}{(\text{Pressure differential, (Pa)})^{0.5}\,(\text{Liquid density, (kg/m}^3))^{0.5}} \qquad \textbf{2.3}$$

$$FN_{US} = 0.66X10^{6} XL^{0.5} X\rho XFN_{SI} \quad \textbf{2.4}$$

A detailed description of different types of nozzles, and their fuel spray characteristics (used in modern combustors to achieve low NO_x emissions) is presented by Lefebvre [26]. This publication also addresses the problem of nozzle coking in greater detail as well as a further discussion about measurement and modeling these characteristics.

2.4 Laser Diagnostics

The laser extinction measurement setup used to determine the soot volume fraction is shown in Figure 2-9. The light source is a Coherent INNOVA 70 series Argon Ion laser that is operated at a wavelength of λ = 514.5 nm. As shown in Figure 2-9, the laser beam is mechanically chopped using a Stanford Research Systems SR530 optical chopper at a frequency of approximately 1000 Hz. The beam then passes through a splitter that directs 30% of the light onto a photodiode, which monitors the laser input. Any fluctuations in the laser beam are monitored using this PIN10DP/SB silicon photodiode, which measures the intensity of a portion of the laser beam I_o. The output of this photodiode is input to a lock-in amplifier. The purpose of using a lock-in amplifier is to eliminate any signal, which does not correspond to the chopped frequency of 1000 Hz. Thus, it helps in filtering out the intensities caused by flame luminosity or any other source. Remaining 70% of the light is directed onto a collimator. The beam after passing

through the collimator, subsequently passes through the two quartz windows of dimensions 6.35 mm diameter by 6.35 mm thick. These windows are located 248 mm downstream from the dump plane. They are placed in a stainless steel housing that was simply fastened to the 51 mm section, as shown in Figure 2-6, of the combustor. These housings utilize Swagelok® components and Teflon gaskets to produce an air tight seal on either side of each quartz window piece. In order to prevent soot deposition on the quartz windows and avoid overheating of the windows, a nitrogen purge is used. The flow rate of nitrogen is measured using an orifice plate with a hole of approximately 0.6 mm in diameter. This nitrogen flow is simply dumped into the combustion chamber after cooling the quartz windows. Since, this nitrogen is added to the existing combustion products, the emission measurements are corrected for this additional nitrogen flow rate, which is measured by monitoring the upstream pressure of an orifice plate of approximately 0.6 mm in diameter. The procedure for emission measurement correction is explained in detail in section 2.6.2.

After passing through the chamber, the laser beam is directed onto another Model PIN-10DP/SB silicon photodiode. This photodiode generates a voltage proportional to the transmitted laser intensity I that is subsequently input to a Stanford Research Systems Model SRS530 lock-in amplifier. Any fluctuations associated with the laser output are eliminated by taking the ratio of I over I_o. These signals are acquired using a National Instruments data acquisition card and are processed using a LabVIEW® application program.

The soot volume fraction (f_v) is obtained using Rayleigh's approximation. This approximation assumes that the ratio of the particle diameter to the wavelength of light is less than 0.3. The refractive index of soot (m) used to determine the soot volume fraction is presented by Smith and Shaddix [27] and is equal to 1.570-0.56*i* for visible wavelengths (λ). Mean soot volume fraction, f_v is given by Equation 2.5 [29, 30].

$$f_v = \frac{\lambda(k_{ext})}{(6\pi)E(m)}$$

2.5

Where, λ is the wavelength of the laser (514.5 nm), E(m) is a function of the index of refraction as shown in equation 2.6.

$$E(m) = -Im\left(\frac{m^2 - 1}{m^2 + 2}\right)$$

2.6

And the extinction coefficient is given by

$$k_{ext} = \left(\frac{\ln\left(\frac{I}{I_o}\right)}{L}\right)$$

2.7

Where, I_o is the intensity of light measured for lean flame conditions where little or no soot is present in the combustion chamber. Note, the I_o is corrected for any fluctuations in the intensity as discussed above.

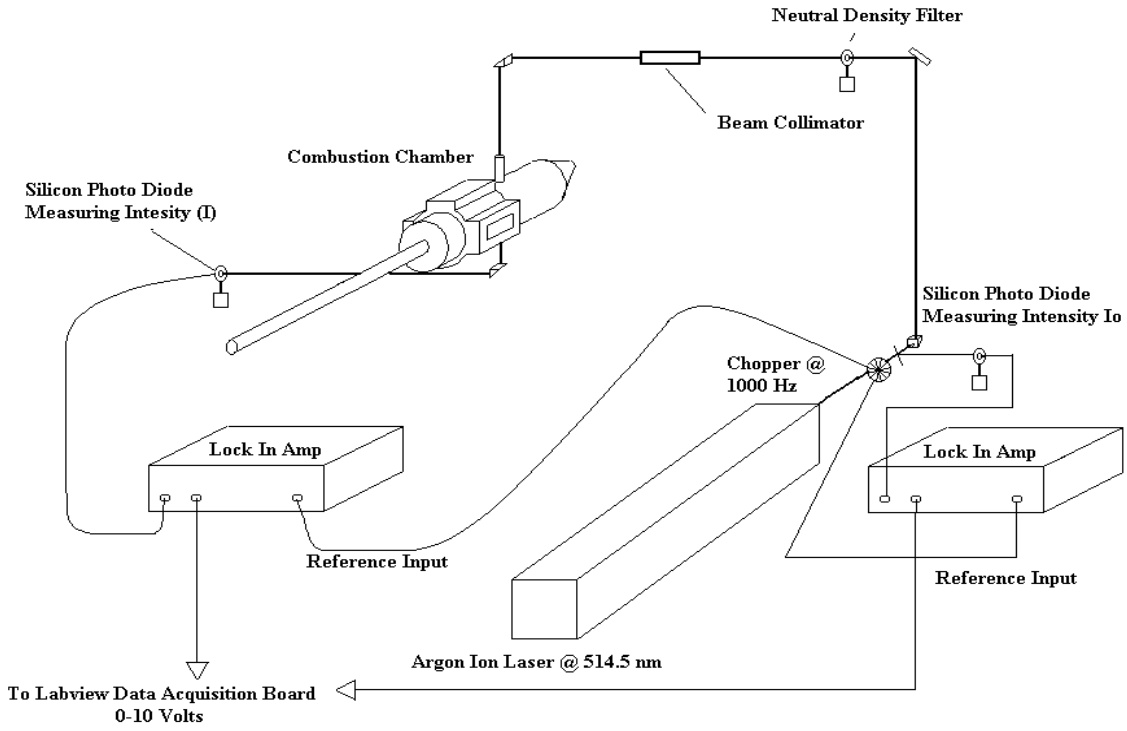

Figure 2-9 Schematic of laser extinction setup for soot measurement

2.5 Data Acquisition System

There are two data acquisition systems, one for low frequency data acquisition rates and the other for high frequency data acquisition rates. The low frequency system consists of two computers. The first of the computers has an A/D convertor (Keithly DAS 1401) board and four expansion (Keithly EXP-16) boards in series. This arrangement provides 64 individual channels. Sampling of experimental data is performed using a custom Visual Basic based program called DASKmaster. The sampling rate is 2 samples per second. All the parameters can be simultaneously monitored during the experiment and this setup also has provisions for recording all the data to a log file. Figure 2-10

shows a typical output display screen for the DASKmaster program. The second computer is used to monitor the laser intensities. It has a (National Instruments BNC 2110) A/D convertor with 8 input channels. The outputs from the lock-in amplifiers (explained earlier in section 2.4) are input into this card. This data is then processed using a LabVIEW® program. The output is stored in a standard output LabVIEW® log file, which can be used for further data analysis.

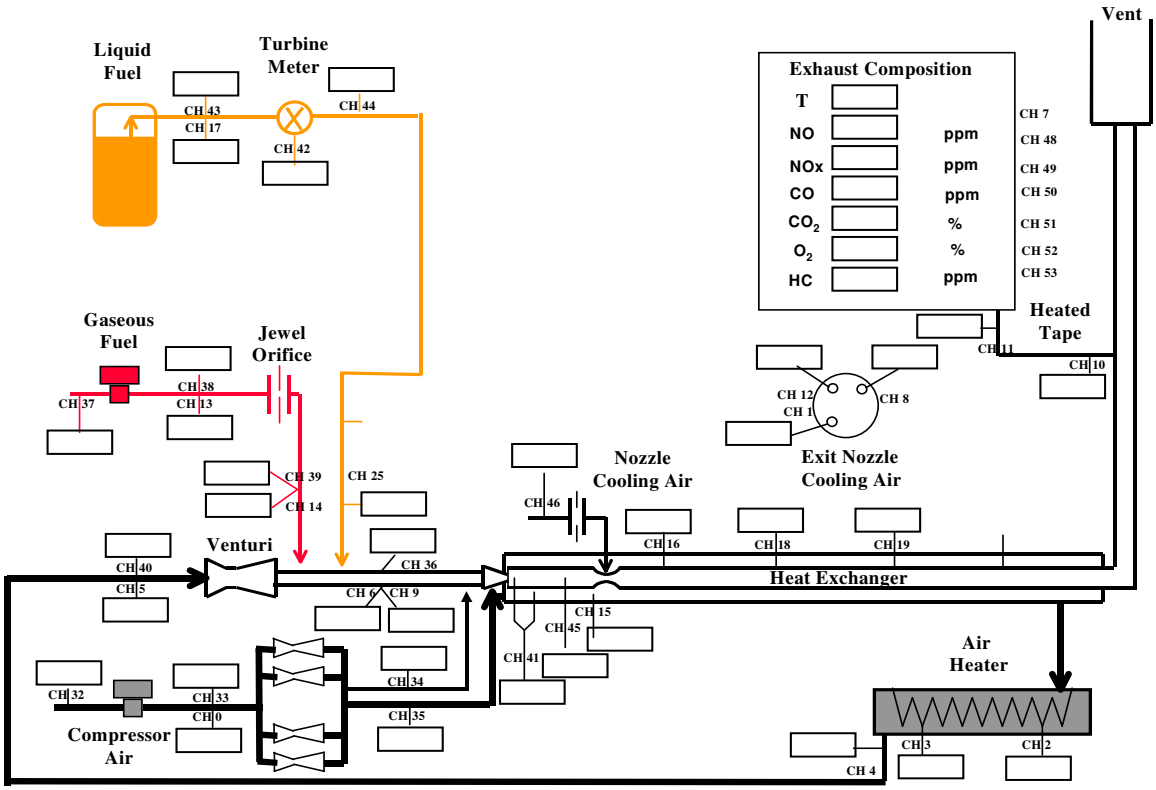

Figure 2-10 DASKmaster output screen

The high-frequency data acquisition system uses a third computer to monitor the PCB piezoelectric transducers (model 113A21) which have a response time of 1 μs. The

model gas turbine combustor has provisions for measurement of the high frequency pressure fluctuations by monitoring the PCB pressure transducers placed at different locations on the combustion chamber. Figure 2-11 shows the location of important PCB transducers. The data acquisition is done using an eight channel A/D sampling board (National Instruments, AT-MIO-16E-1). A sampling rate of 30 KHz is used. The data is collected and processed using a LabVIEW® program.

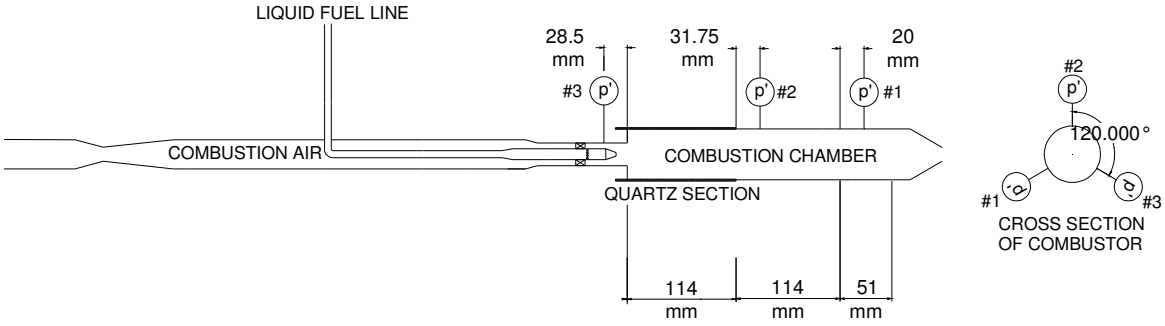

Figure 2-11 Location of PCB transducers

2.6 Emissions Measurement

2.6.1 Sampling System

Figure 2-12 shows the schematic of the exhaust gas sampling system and emission analyzers setup. The exhaust gases are sampled through a probe inserted inside the exhaust tube. A vacuum pump draws exhaust gas through an ice bath and water trap, consequently, removing any moisture in the exhaust gas. In addition, a filter is used to remove any particulate matter (PM) present in the exhaust gas that is located upstream of

the vacuum pump. The sample gas is further directed into the analyzers at specified flow rates and excess amount of sample gas is bypassed through the vent. The exhaust gas sampling system consists of a non-dispersive infrared CO (Horiba) analyzer, CO_2 (Beckman) analyzer, a paramagnetic O_2 (Beckman) analyzer and a Chemiluminescence NO_X (Thermo Environmental Instruments) analyzer. Appropriate calibration gases are used to calibrate these analyzers before and after the test in order to check for drift in emission measurements.

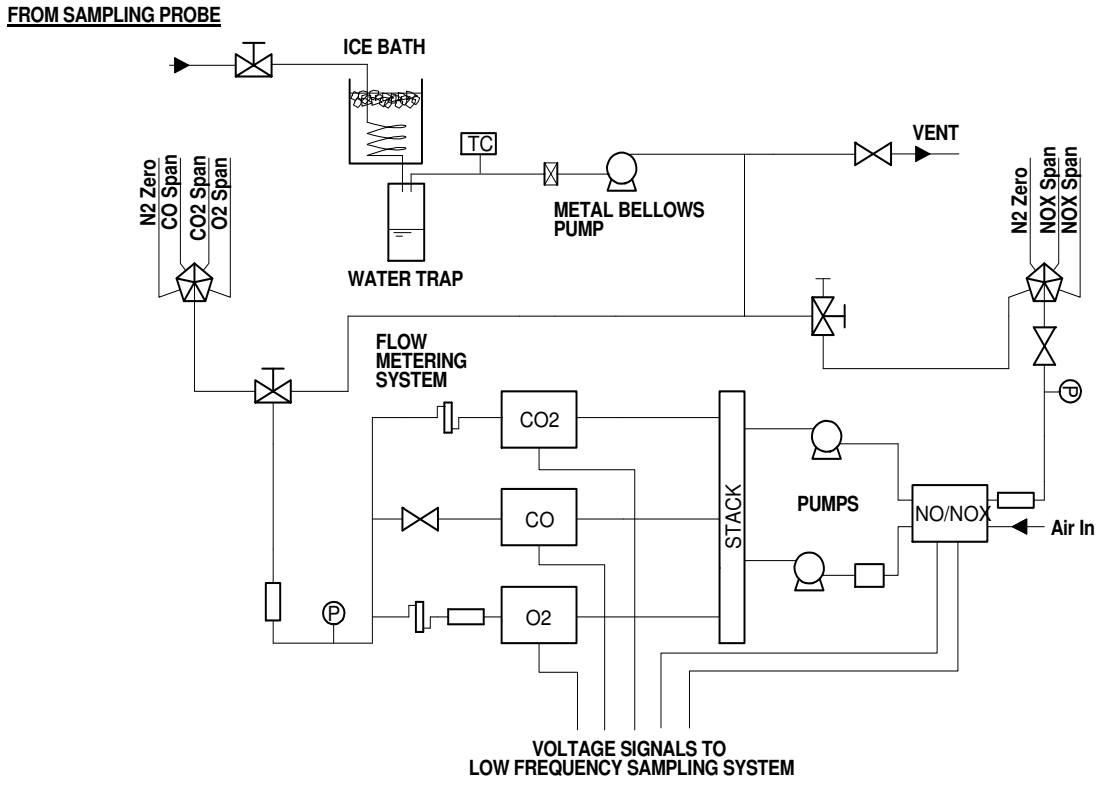

Figure 2-12 Exhaust gas sampling and emissions analyzer setup

Table 2-1 tabulates the analyzer ranges used for the experiments and the specified uncertainties. Outputs from analyzers are sampled by the low-frequency data acquisition

system described in section 2.5. The voltages thus obtained are converted to the concentration by the use of appropriate constants by the DASKmaster program.

Table 2-1 Analyzer ranges and uncertainties

Analyzer	Range	Uncertainty
$NO\text{-}NO_x$	0-1000 ppm	$\pm$ 1% FS
CO	0-1000 ppm	$\pm$ 1% FS
O_2	0-25%	$\pm$ 1% FS
CO_2	0-20%	$\pm$ 1% FS

2.6.2 Emission Corrections

Emission products are diluted by the nitrogen cooling purge used for the quartz windows and nozzle cooling air hence, a correction factor is required in order to calculate the actual molar concentrations of each species. This factor can be calculated as follows. Consider combustion of an arbitrary hydrocarbon at lean conditions assuming no dissociation, which is given by equation 2.8. The equation approximates 79% N_2 and 21% O_2 in the oxidizer, in this case air.

$$C_xH_yO_zN_w + \left(\frac{x + \frac{y}{4} - \frac{z}{2}}{\phi}\right)(O_2 + 3.76N_2) \rightarrow$$

$$xCO_2 + \frac{y}{2}H_2O + \left(\frac{1-\phi}{\phi}\right)\left(x + \frac{y}{4} - \frac{z}{2}\right)O_2 + \left[3.76\left(\frac{x + \frac{y}{4} - \frac{z}{2}}{\phi}\right) + \frac{w}{2}\right]N_2 \qquad \textbf{2.8}$$

The nitrogen purge flow rate is approximately 1 g/s, and the cooling air flow rate is approximately 2.7 g/s. These flow rates are converted to the molar fractions of the combustion air by taking the ratio of each molar flow rate to that of the combustion air molar flow rate as indicated in equations 2.9 and 2.10. It should be noted that the molecular weight terms in equation 2.9 cancel out since the composition of cooling air and combustion air are assumed to be the same.

$$\text{Cooling Air Molar Ratio (CA)} = \frac{\text{cooling air mass flow rate}}{\text{combustion air mass flow rate}} \quad \textbf{2.9}$$

$$\text{Nitrogen Purge Molar Ratio (NP)} = \frac{\text{nitrogen purge mass flowrate}}{\text{combustion air mass flow rate}} \left(\frac{MW_{air}}{MW_{N_2}} \right) \quad \textbf{2.10}$$

The total number of moles of the cooling air and the nitrogen purge can be expressed as a fraction of the total number of moles of the combustion as indicated by Equations 2.11 and 2.12 respectively.

$$N_{CA} = CA \left(\frac{x + \frac{y}{4} - \frac{z}{2}}{\phi} \right) (O_2 + 3.76N_2) \quad \textbf{2.11}$$

$$N_{NP} = NP \left(\frac{x + \frac{y}{4} - \frac{z}{2}}{\phi} \right) (O_2 + 3.76N_2) \quad \textbf{2.12}$$

As observed from Figure 2-5, the distance between the exhaust nozzle and the analyzer sampling probe is large. Hence, there exists a possibility of further reactions

between the products of combustion but, the introduction of the nozzle cooling water, as discussed earlier, ensures that temperature of the exhaust gases is well below the temperature required to induce any further chemical reactions. Therefore, it can be assumed that the composition of exhaust gases between the nozzle outlet and the analyzers is unchanged.

Further, the correct molar concentration of a species in the exhaust stream can be calculated by subtracting the molar concentration, X_i", of that species added due to cooling air from the total concentration that is recorded by the analyzers ,X_i'. This corrected concentration is further used to calculate the total number of moles of species, i, in the exhaust stream by multiplying it with the total number of dry moles N_t (dry). Further, the total number of moles of species, i, are divided by the total number of moles of the dry combustion products N_t (combustion) to obtain the corrected molar concentration of species, i, in the combustion products only.

Equations 2.13 through 2.15 are used to calculate the corrected molar concentration of species, i, in combustion products.

$$N_{t,\,dry} = \left(x + \frac{x + \frac{y}{4} - \frac{z}{2}}{\phi}\right)\left[4.76(1 + CA + NP) - \phi\right] + \frac{w}{2}\right) \qquad \textbf{2.13}$$

$$N_{t,\,combustion} = \left(x + \frac{x + \frac{y}{4} - \frac{z}{2}}{\phi}\right)\left[4.76 - \phi\right]\right)$$

2.14

$$X_{i,\,\text{corrected}} = \left(\frac{(X_i' - X_i'')(N_{t,\,\text{dry}})}{N_{t,\,\text{combustion}}} \right)$$

2.15

Equation 2.15 gives the corrected molar concentration of species, i, but this concentration must be corrected to 15% O_2 level since this is a standard procedure for reporting emissions for the combustion devices. This also ensures uniformity in results irrespective to the different combustion environments. Equation 2.16 shows the standard correction procedure.

$$X_i \text{ (corrected to 15\% } O_2) = X_i \text{ (from Eq 2.15)} \left(\frac{N_{\text{mix,dry}} \text{ @ analyzed } O_2\,\%}{N_{\text{mix,dry}} \text{ @ 15\% } O_2} \right)$$

2.16

Where, $N_{mix,\ dry}$ is the total number of dry moles in the combustion products calculated using equation 2.17 expressed as a mole fraction of oxygen for any hydrocarbon.

$$N_{\text{mix, dry}} = 4.76 \left[\frac{x + (1 - \chi_{O_2}) \left(\frac{y}{4} + \frac{z}{2} \right) + \frac{w}{2} \chi_{O_2}}{\left(1 - 4.76 \chi_{O_2} \right)} \right] - \frac{y}{4} + \frac{w}{2}$$

2.17

Chapter 3

Results and Discussion

This section presents an overview of the results obtained in the current study.

3.1 Characterization of Fuels

A series of studies were performed using candidate jet fuels JP-8, JP-900, Fischer-Tropsch (FT), and JP-8/FT blends with the purpose of comparing them to current fuel used by the military gas turbine engines, JP-8. The measurements of hydrogen to carbon (H/C) ratio, smoke point, heat of combustion and composition were obtained, which are discussed next.

3.1.1 Hydrogen to Carbon Ratio Measurements.

Hydrogen to carbon (H/C) ratio for a fuel is required to calculate the overall equivalence ratio. These H/C ratios were obtained following the procedure described in the ASTM standard D 5373-08 [30]. The instrument used for H/C measurements was a LECO Truspec Carbon, Hydrogen, and Nitrogen analyzer, which accepted a 30-40 mg sample of the fuel. In this instrument all of a hydrocarbon fuel is converted to carbon dioxide and water, while the nitrogen-containing species to nitric oxides. The reproducibility of this method is approximately 1%. No nitrogen was detected in any of the fuels tested. Table 3-1 tabulates the mass of the sample tested, the mass percentages

of carbon and hydrogen, the molar H/C ratio, and the percent mass recovered. The calculated H/C ratios are: 1.84 for JP-900; 1.94 for JP-8; and 2.13 for the FT fuel.

Table 3-1 Hydrogen to carbon ratio measurements

Fuel	Batch numbers	Sample mass(g)	C%	H%	H/C ratio	% Mass recovered
JP-900	PA 67-132-5	0.0365	83.8	12.9	1.85	96.7
		0.0361	84.7	12.9	1.83	97.6
JP-8	UN 1863	0.0398	82.2	13.3	1.94	95.5
		0.0378	82.7	13.3	1.93	96.0
FT	Syntroleum S-8 (5109)	0.0384	81.6	14.6	2.15	96.2
		0.0332	82.9	14.7	2.13	97.6
		0.0411	82.3	14.5	2.11	96.8

3.1.2 Smoke Point Measurements

Smoke point is defined as the maximum height of the diffusion flame, which is just below the point where the flame begins to produce smoke, measured on a standard apparatus under reproducible conditions. It provides an indication of the relative sooting tendency of the fuels. Fuels with lower smoke points tend to produce more soot and vice versa. For the case of aviation gas turbine fuels, U.S. Air Force has established a specification that requires a minimum smoke point of 19 mm [10]. For liquid fuels such as kerosene and jet fuels, ASTM D-1322 [31] defines the procedure for measuring smoke points up to 50 mm flame lengths on the standard wick-fed apparatus. Following this procedure, smoke point measurements are reported in Table 3-2 for JP-8, JP-900, FT and also for one 50/50% by volume blend of JP-8 and FT.

Table 3-2 Smoke point measurements

Fuel	Batch Number	Smoke Point (mm)
JP-8	UN 1863	21.3
JP-900	PA 67-132-5	22.1
FT	Syntroleum S-8 (5109)	>50
JP-8/FT blend (50/50)	UN 1863/5109	29.0

Generally, it is observed that the fuels with higher aromatic content such as JP-8 will have a lower smoke point and this trend is evident in the smoke point measurements. As an alkane-rich fuel, FT contains virtually no aromatics. In fact, the smoke point of the FT fuel was too high to be measured using the standard apparatus. Therefore, it would be expected that the FT burns more cleanly and should produce very little soot in the model gas turbine combustor. JP-8 and JP-900, in contrast, have lower smoke points and, therefore, would be expected to produce more soot. The JP-8/FT (50/50) blend smoke point, 29 mm, falls between the smoke points of JP-8 and FT separately and, therefore, should produce less soot than JP-8. All of the fuels tested meet the 19 mm minimum in jet fuel specifications.

Often, Threshold sooting index (TSI) is also used to characterize the sooting tendency of hydrocarbon fuels. TSI gives a relation between molecular weight of fuel and respective smoke points. Mensch [32] presented a detailed work that relates the sooting tendency of pure compounds and JP-8 with the TSI values. In this study TSI was calculated using Equation 3.1.

$$TSI_{meas} = a\left(MW_{fuel}/SP_{fuel}\right) + b \qquad \textbf{3.1}$$

Where, a = 4.07 mm*(g/mol)$^{-1}$ and b = - 4.8.

Using this expression a rough estimate of TSI is obtained for JP-8, JP-900 and FT fuels in current study and these are presented in Table 3-3. The molecular weight used for calculating the TSI values are estimated as follows. For JP-8, the molecular weight is predicted for the average composition that is presented by Edwards *et al.* [10]. For JP-900, molecular weight of decalin (trans-decahydro naphthalene) is used since it is a single major compound found in JP-900, which is discussed ahead in section 3.1.3. Further, molecular weight of undecane is used to calculate the TSI for FT fuel since this fuel shows a broader distribution of compounds from octane to pentadecane,, which is discussed ahead in section 3.1.3. The molecular weight of undecane represents an average for an assumed equal distribution of these compounds.

Table 3-3 Estimated TSI values for fuels studied

Fuels	MW (g/mol)	SP (mm)	Measured TSI
JP-8	153.3	21.3	24.49
JP-900	138.25	22.1	20.66
FT	156.31	>50	<7.92

It is important to note that higher TSI values indicate higher sooting tendency. From the estimated TSI values obtained above it is observed that FT fuel has considerably lower value compared to JP-8 and JP-900 and thus would produce lower

soot volume fraction in the combustor as compared to these fuels. However, the sooting tendencies of JP-8 and JP-900 cannot be distinguished based on the estimated TSI values since the difference in these values is not very large.

3.1.3 Composition Measurements

Gas chromatography (GC-MS) analysis was performed for the three fuels studied. The instrument used for obtaining these chromatographs was a Shimadzu QP-5000 analyzer. From the GC-MS analyses results the major components of the fuels can be identified.

The chromatogram for JP-8 is presented in Figure 3-1. In this figure, major peaks correspond to alkanes and iso-alkanes (iso-paraffins) with smaller quantities of cyclo-alkanes and benzene derived compounds. Alkane and iso-alkane peaks correspond to compounds ranging from C_7 (heptane) through C_{16} (hexadecane). Additionally, peaks labeled 1 through 5 represent the smaller quantities of cyclo-alkanes present in JP-8. As discussed earlier, polycyclic aromatic hydrocarbons (PAH) promote soot production and JP-8 does contain aromatic compounds such as 1, 2, 3 tri-methyl benzene and 1, 2 di-methyl, 4 ethyl benzene. Therefore JP-8 is expected to produce more soot, which is also evident from the smoke point measurements.

Further, JP-900 shows dominant peak of trans-decahydro naphthalene (Figure 3-2), unlike JP-8, which shows a broader distribution of the compounds. Apart from this peak, the overall composition of JP-900 includes smaller quantities of saturated cyclic

compounds ranging from C_7 (methyl-cyclohexane) to C_{14} (tetradecahydro-anthracene). Very small amounts of aromatic compounds were found in JP-900 as compared to JP-8.

Unlike JP-8 and JP-900, FT fuels lack aromatic content and saturated cyclic hydrocarbons. Figure 3-3 shows a distribution of straight-chained alkanes and iso-alkanes ranging from C_8 (octane) to C_{15} (pentadecane). Branches on iso-alkanes are mainly comprised of methyl and ethyl groups. Thus, this fuel is expected to exhibit lower sooting characteristics in model gas turbine combustor compared to JP-8 and JP-900.

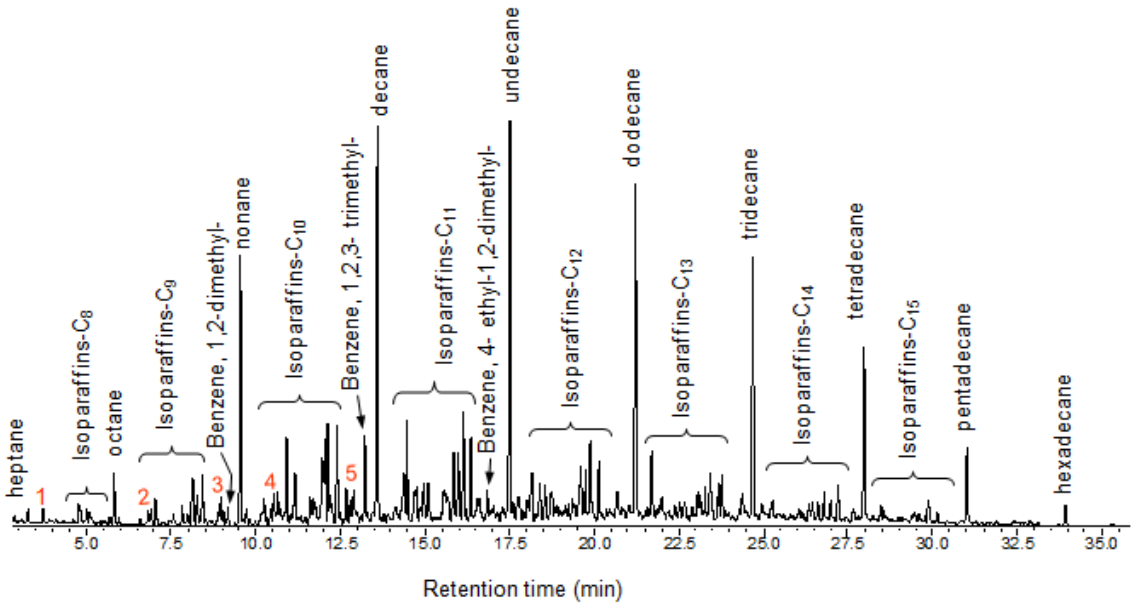

Figure 3-1 Gas chromatogram of JP-8 (UN 1863), peaks labeled from 1 through 5 correspond to the following cyclo-alkanes: 1. methyl-cyclohexane, 2. ethyl-cyclohexane, 3. 1-ethyl-4-methyl-cyclohexane, 4. propyl-cyclohexane, 5. 1-methyl-3propyl-cyclohexane

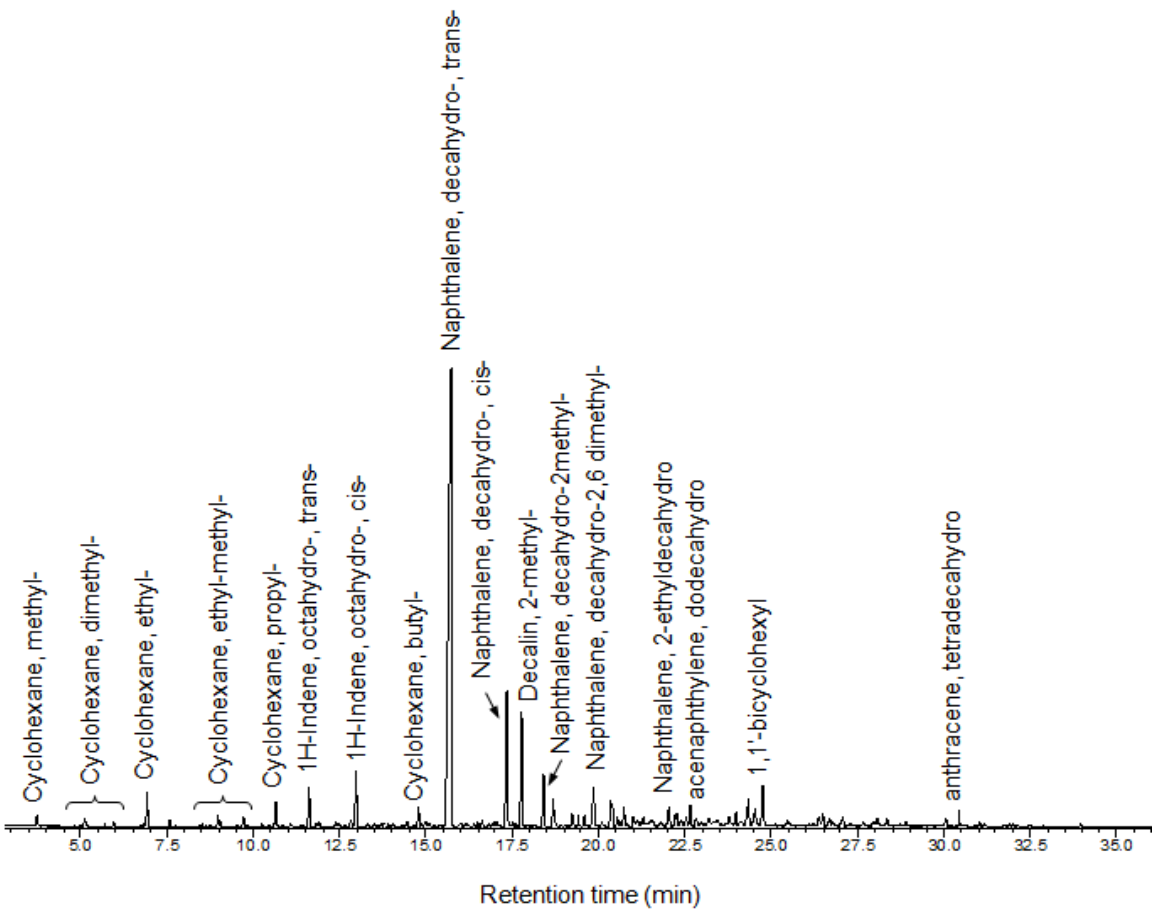

Figure 3-2 Gas chromatogram of JP-900 (PA 67-132-5)

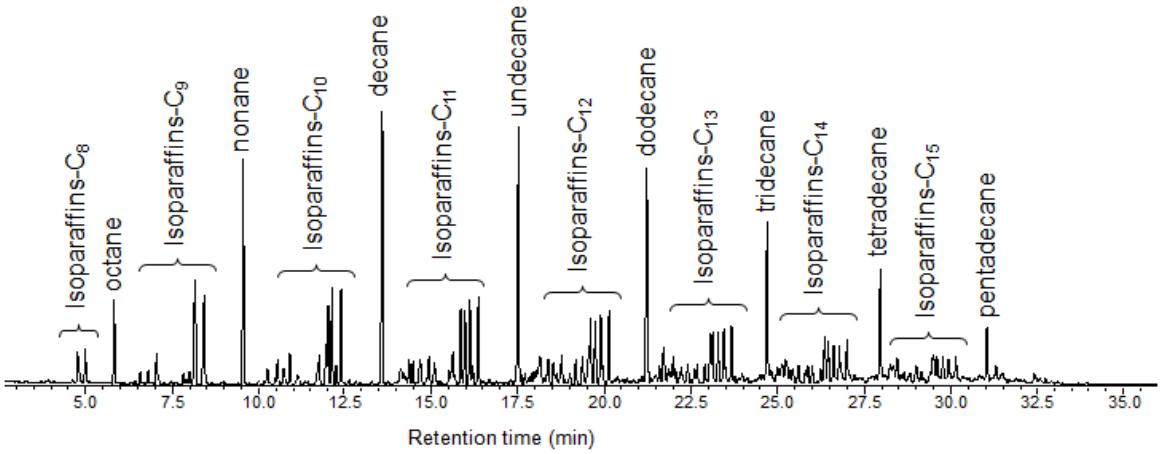

Figure 3-3 Gas chromatogram of Fischer-Tropsch (Syntroleum S-8 5109)

3.1.4 Heat of Combustion Measurements

In order to use alternative fuels in existing combustors, it is necessary to compare the heat of combustion of alternative fuels with the existing fuel, in this case, JP-8. The heat of combustion measurements were made using a Parr 1261 calorimeter and Parr 1563 water handling system at the Bucknell University. Calibrations were performed on this instrument using benzoic acid to ensure correct measurements. Results of the heat of combustion measurements are presented for the higher heating values (HHV) in Table 3-4.

Table 3-4 Heat of combustion measurements

Fuel	Batch Number	HHV (MJ/kg)	HHV (Btu/lbm)
JP-8	UN 1863	45.91± 0.18	19738.62 ± 79.34
JP-900	PA 67-132-5	45.51 ± 0.09	19564.59 ± 39.97
FT	Syntroleum S-8 5109	47.16 ± 0.17	20274.10 ± 75.21

Fuel	ρ (kg/m^3)	LHV (MJ/kg)	LHV (Btu/lbm)
JP-8	784.5	43.09	18525.26
JP-900	849.7	42.77	18387.73
FT	728.1	44.08	18951.27

Previous work has shown that the lower heating value (LHV) for JP-8 jet fuel is 43.15 MJ/kg (18550 Btu/lbm) [10]. To facilitate the comparison between the literature value (LHV) of JP-8 and the higher heating values (HHV) obtained using calorimeter, it

is necessary to convert the calorimeter values to their respective LHV. This was achieved following the ASTM standard D 240 [33]. This standard specifies the method for converting the HHV into the LHV with the use of mass percentage of hydrogen in the fuel that is acquired from the H/C ratio measurements discussed earlier. Subsequently, it is observed that the LHV obtained using this conversion for JP-8 (UN 1863), 43.09 MJ/kg (18525.26 Btu/lbm), is very close to the value reported by Edwards *et al.* [10]. JP-900 shows similar energy content; on the other hand, FT fuel provides slightly higher heat of combustion than JP-8. It is worth noting that FT fuels have a lower density than either JP-8 or JP-900, which offsets the higher heat of combustion for volume limit applications.

3.2 Combustion Stability, Soot and Emissions Results

3.2.1 Experimental conditions

In order to compare the results between different runs of all the fuels, the model combustor was run at constant air inlet temperature and constant flow rate of air conditions, which are presented in Table 3-5. The inlet temperature was measured at a location upstream of the critical venturi (see Figure 2-5) and was kept constant at 550K $\pm$ 10K. The chamber was operated at a mean pressure of 0.51 MPa. The equivalence ratio was changed by increasing/decreasing the liquid fuel flow rate, while the air flow rate was kept constant at 32 g/s. The range of equivalence ratio typically varied from $\phi = 0.5$ to $\phi = 1.4$ over the course of the liquid fuel experiments. The uncertainty introduced in

equivalence ratio measurement due to the uncertainty in instrumentation (discussed in Appendix A) is approximately $\phi \pm 2.60\%$, which approximately converts to $\phi = \pm 0.02$.

Table 3-5 Experimental running conditions

Parameters	Values
Air mass flow rate	32 g/s
Inlet temperature (T_{up})	550 K
Injector	Peanut (Delavan pressure atomizer) Flow number 1.9 spray angle 85^0
Chamber pressure, P_c	0.51 MPa
Swirl angle	45^0
Chamber length, L_c	307 mm

Since, the exhaust nozzle of the combustor is water-cooled; there is no provision to measure combustor exit temperature. Therefore, all results of the combustion studies are presented as a function of measured value of equivalence ratio at a constant inlet temperature.

3.2.2 Combustion Stability

The stability map of the fuels is presented in Figure 3-4 with the ordinate representing the root mean square (rms) value of the recorded pressure fluctuations, measured by a transducer located 248 mm from the dump plane of the combustor normalized by the mean chamber pressure, P_c. The results indicate that these fuels burn stable (pressure fluctuations < 1%) for most of the cases. It is also observed that pressure

fluctuations exceed a value of 2% for two instances for one of the JP-8 runs and a JP-900 run, however, no discernable trend was observed.

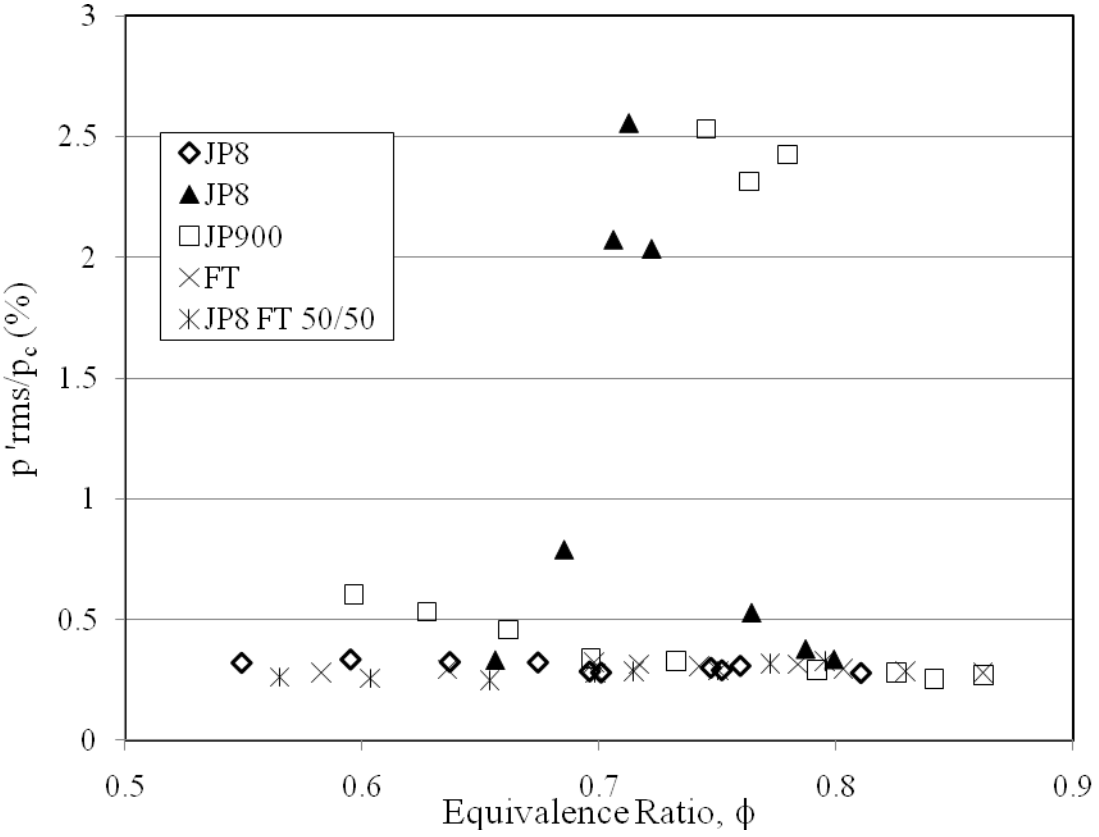

Figure 3-4 Combustion stability results for different fuels and blends as a function of equivalence ratio

In a similar study, Mordaunt *et al.* [34] presents a comparison for instability measurements for fuels JP-8, HDT RCO/LCO (1:1), n-heptane. A notable difference in these measurements as compared to the present instability results is that pressure oscillations of up to 10% were observed. However, the conditions where combustion instability was observed, the air inlet temperatures were much higher (~ 670 K) and a different spray injector geometry was used. As combustion instability is very sensitive to

boundary and initial conditions, slight changes in inlet air temperature or fuel nozzle geometry, which affects mixing and spray atomization process, could influence the combustion instability behavior [35]. In addition, Lee *et al.* [15] have also shown that coal-based fuels show pressure fluctuations of the order of 1% in a study conducted earlier with same kind of injector and combustor setup, which leads to the assertion that all fuels studied burn stably.

3.2.3 Soot Volume Fraction Results

Figure 3-5 shows the mean soot volume fraction data obtained for JP-8, JP-900, FT, and the JP-8/FT (50/50), (25/75) blends in model gas turbine combustor. The ordinate represents the soot volume fraction in ppm and the abscissa represents equivalence ratio.

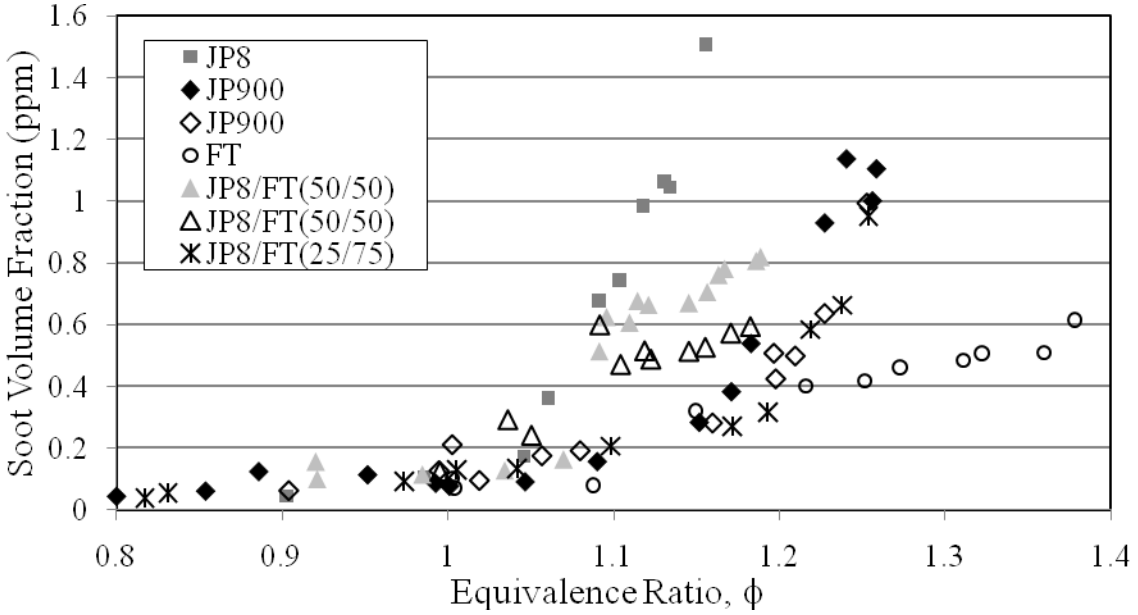

Figure 3-5 Soot volume fraction results for different fuels and blends as a function of equivalence ratio

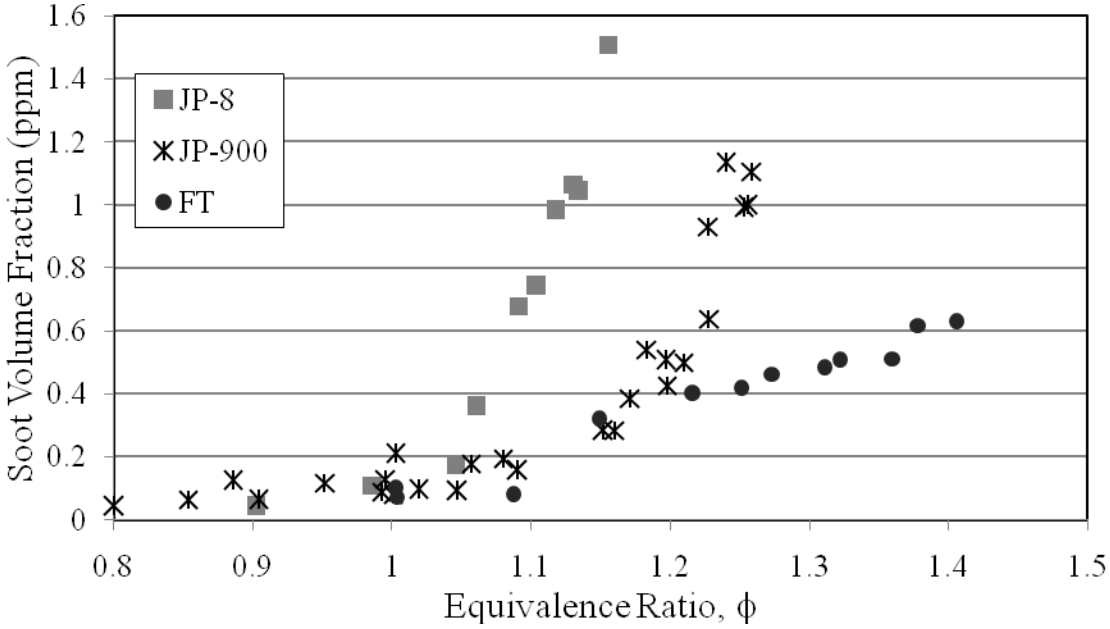

Figure 3-6 Soot volume fraction results for JP-8, JP-900 and FT fuels as a function of equivalence ratio (2 runs of JP-900 results are presented together)

Note that for the JP-900 and JP-8/FT (50/50) two separate runs are included on the figures. This allows some comparative data on the reproducibility of the data. To simplify the interpretation of these results the data presented in Figure 3-5 is segregated and presented in three additional figures.

As observed in Figure 3-5, all the fuels produce negligible amounts of soot below an equivalence ratio of $\phi = 1.05$. Figure 3-6 shows a comparison of JP-8, JP-900 and FT fuels. Results obtained for both JP-900 runs are presented together. In this figure, it is observed that all fuels produce very low soot up to an equivalence ratio of $\phi = 1.05$. However, the mean soot volume fraction of JP-8 shows a prominent rise above this equivalence ratio. On the other hand, JP-900 and FT indicate low sooting propensity up to an equivalence ratio of approximately $\phi = 1.15$ above which JP-900 shows a notable

rise as compared to FT. Thus, the results clearly indicate that JP-8 produces higher amounts of soot in model gas turbine combustor at richer conditions compared to JP-900 and FT. In contrast, FT has shown very low volume fractions even at rich conditions ($\phi >$ 1.3). As compared to JP-8, JP-900 has indicated lower soot volume fraction and its trend lies in between the trends of JP-8 and FT. The reason for the difference observed between JP-8 and FT fuels is simply a consequence of the high alkane and iso-alkane content in FT. Alkanes are well known to produce smaller amounts of soot as compared to aromatic species, which JP-8 can contain up to 20%. The difference between JP-8 and JP-900 is less easy to explain. As it is noted earlier, JP-900 indicated a composition, which comprised of higher percentage of cyclo-alkanes with little or no aromatics content. The presence of saturated cyclo-alkanes may delay the onset of particle inception and surface growth. McEnally and Pfefferle [36] have studied the decomposition of cyclohexane introduced as a dopant in highly diluted methane/air diffusion flame. In this work, the cyclohexane is observed to undergo unimolecular dissociation to form C_2, C_3 and C_4 hydrocarbons. Furthermore, production of soot for cyclohexane (in terms of soot volume fraction) is similar to the production observed in linear alkanes such as heptanes [36, 37]. If we extend these findings to cyclo-alkanes in general then JP-900 should form soot in a manner similar to an alkane fuel such as FT. In fact, this phenomenon is observed in the present studies.

Further, Figure 3-7 shows a comparison of mean soot volume fraction obtained for JP-8 and JP-8/FT blends. The results obtained for both JP-8/FT (50/50) runs are combined for illustrating the reproducibility of the results. In this figure, it is observed

that JP-8 and JP-8/FT (50/50), (25/75) blends show low mean soot volume fractions up to an equivalence ratio of $\phi = 1.05$. Above this equivalence ratio, JP-8 and JP-8/FT (50/50) blend show considerable rise as compared to JP-8/FT (25/75) blend. On the other hand, the mean soot volume fraction obtained for JP-8/FT (25/75) blend remains low up to an equivalence ratio of about $\phi = 1.2$ and shows a prominent rise above it. From this figure it is clear that blending JP-8 with FT can reduce mean soot volume fraction in a combustor operating rich. The presence of JP-8 in FT fuel would also assist in improving the poor seal swell characteristics of FT, as discussed earlier, by the introduction of aromatic content. Thus the addition of FT to JP-8 improves the sooting characteristics as compared to JP-8 while the presence of JP-8 helps preserve the seals in the engine [21]. It is worth pointing that Jet-A/FT (50/50) [23, 24] blends and JP-8/FT (50/50) blends have recently been approved for the use in both commercial and military aircrafts.

Figure 3-8 shows the mean soot volume fractions obtained for JP-900 and JP-8/FT (50/50) blend. For JP-900, the reproducibility of data is good. It is also observed for JP-8/FT (50/50) trend that there is considerable scatter, especially at rich conditions.

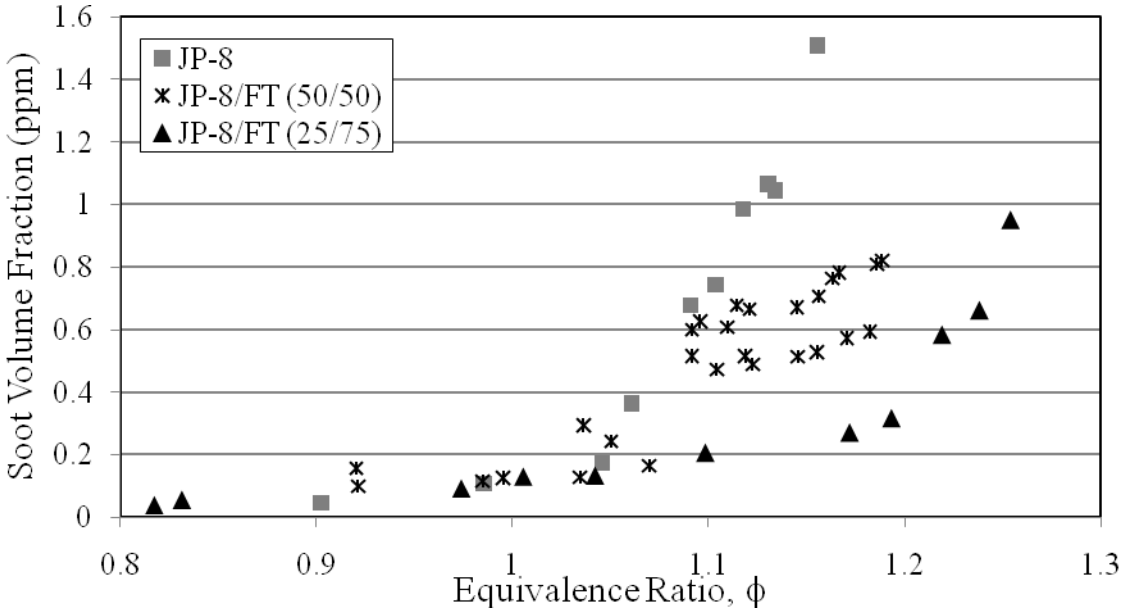

Figure 3-7 Soot volume fraction results for JP-8 and JP-8/FT blends (2 runs of JP-8/FT (50/50) blend are presented together)

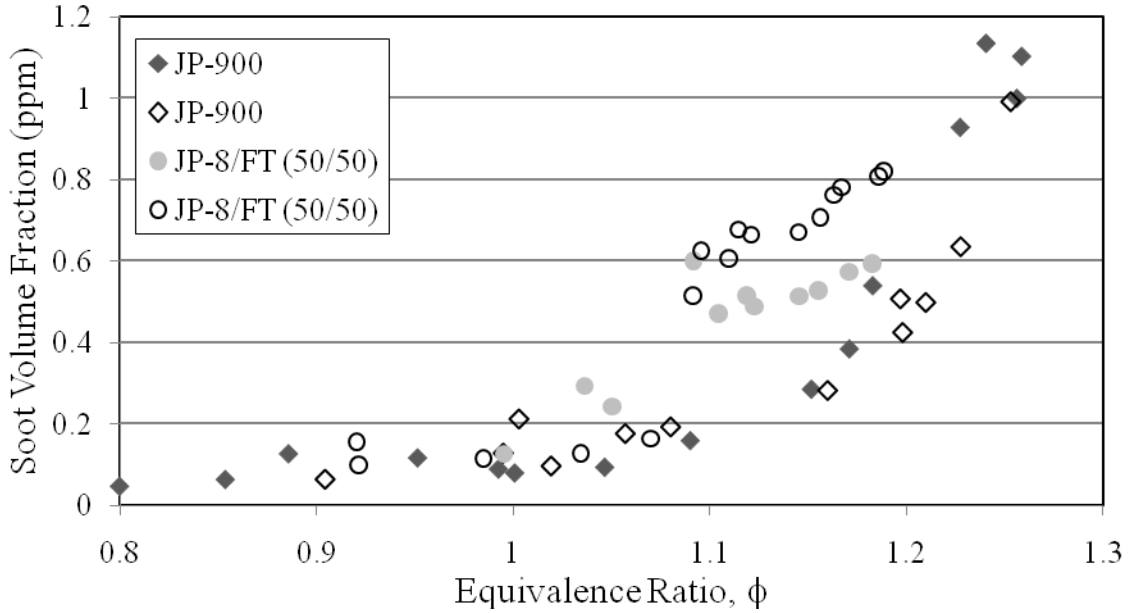

Figure 3-8 Soot volume fraction results for JP-900 and JP-8/FT blend as a function of equivalence ratio

3.2.4 Emissions Measurements

Emission measurements of NO_x and CO were obtained in a separate series of experiments from the soot measurements. In order to increase the level of confidence in the liquid fuel emission measurements, a series of CNG emission data points were acquired at matching inlet conditions before and after all liquid fuel experiments. These measurements helped in checking any drift in the emission analyzers over the duration of the experiment. Appendix B.1 provides the details of these measurements obtained for CO and NO_x analyzers for different fuels and blends. Additionally, all the analyzers were calibrated with known concentration of calibration gases before the experiments and these calibrations were reconfirmed at the end of the experiments. It is important to note that the emission measurements are limited to $\phi < 0.9$ due to a possibility of choking the PM filter, which is located upstream of the vacuum pump used for sampling the exhaust gas, at higher equivalence ratios.

3.2.4.1 NO_x Emissions

The results for NO_x emissions for various fuels and blends are presented in Figure 3-9. The ordinate in this figure represents the NO_x concentration in ppm and the abscissa represents the equivalence ratio. All the emissions are corrected to 15% O_2 level. Note that FT, JP-8 and JP-8/FT (50/50) runs are repeated to compare the reproducibility of the results. To simplify the interpretation of these results, the data presented in Figure 3-9 is segregated and presented in three additional figures.

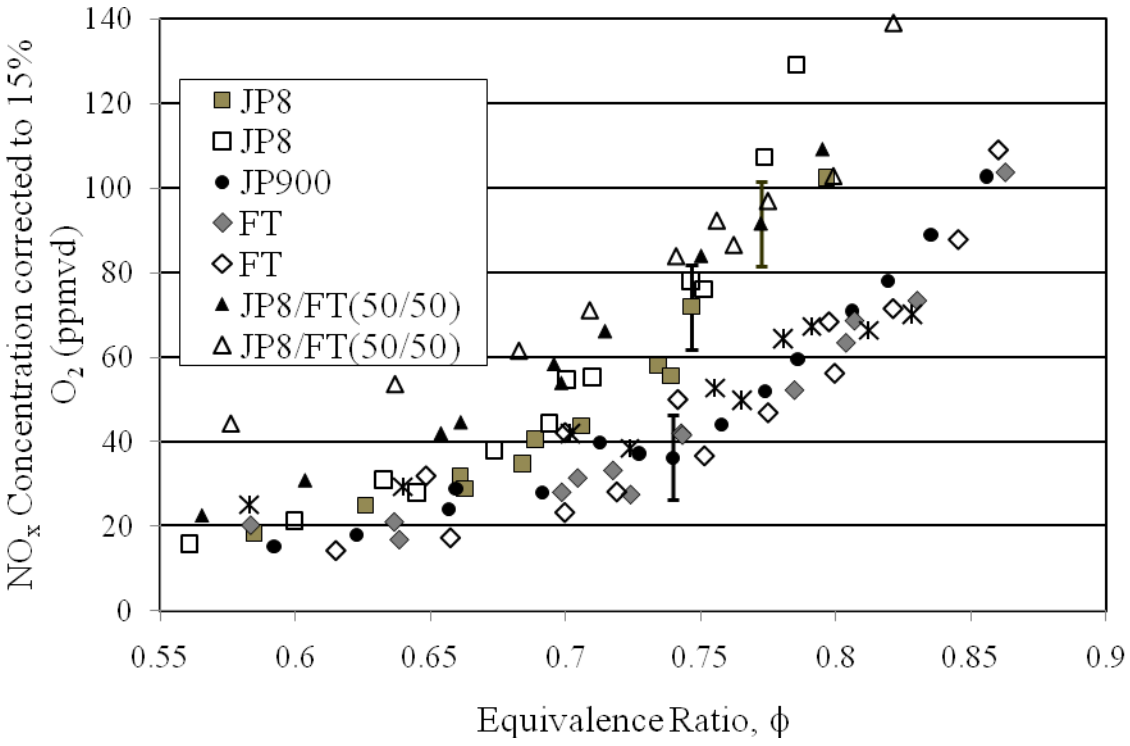

Figure 3-9 NO_x emission results for different fuels and blends as a function of equivalence ratio

Figure 3-10 presents the NO_x emission data for JP-8, JP-900 and FT fuels. These results indicate that, for the same inlet conditions, JP-900 and FT produce lower NO_x compared to JP-8. In addition, it can be observed that JP-900 and FT show results of similar magnitude considering the instrument uncertainty ($\pm$ 10 ppm), as discussed earlier. Further, JP-8 shows a notable rise in NO_x emissions above an equivalence ratio of $\phi \sim 0.75$. This sudden rise indicates that the thermal NO_x production rates increase significantly as flame temperature approaches approximately 1800 K (Note that based on equilibrium calculations these fuels and blends have nearly identical adiabatic flame temperatures). Figure 3-11 presents the comparative NO_x emission data for JP-8 and JP-

8/FT blends. The results shown in this figure indicate that JP-8 has higher NO_x and is similar to JP-8/FT (50/50) blend. On the other hand, JP-8/FT (25/75) blend shows lower NO_x emission.

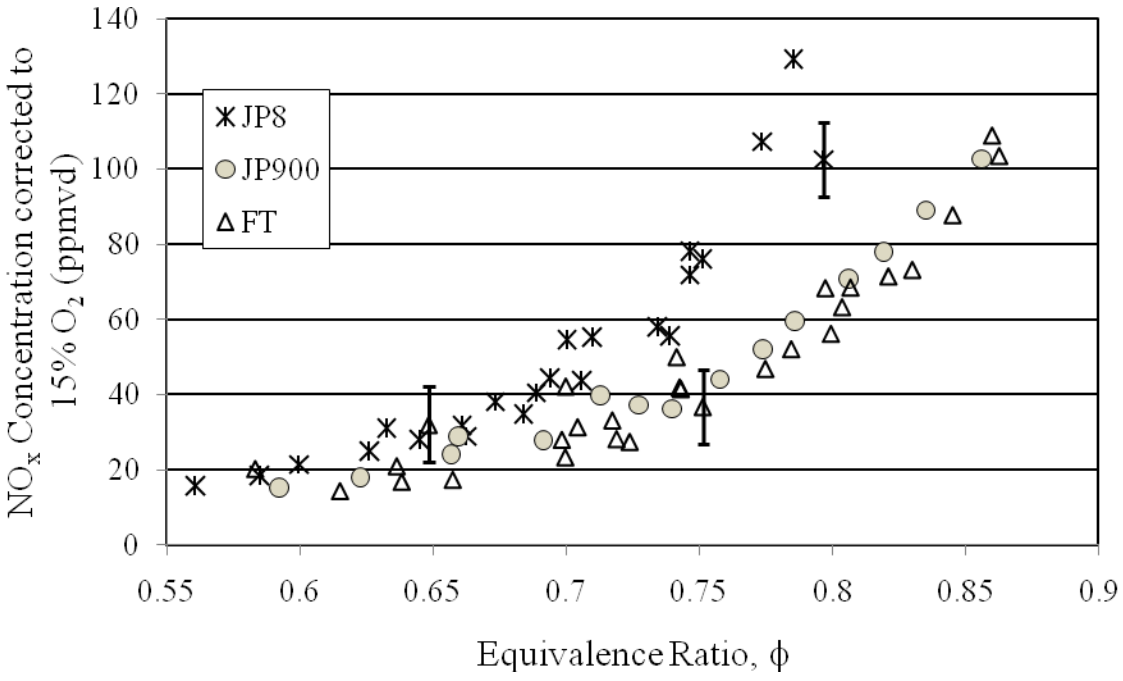

Figure 3-10 NO_x emission results for JP-8, JP-900 and FT fuels as a function of equivalence ratio (2 runs of JP-8 and FT are presented together)

To examine the reproducibility for fuels and blends containing JP-8, runs of JP-8, JP-8/FT (50/50) blend and FT were repeated. Figure 3-12 presents a comparative study of the reproducibility data obtained for JP-8, JP-8/FT (50/50) and FT fuel. In this figure, FT shows good reproducibility between runs as compared to JP-8 and JP-8/FT (50/50) blend. For JP-8, significant scatter in data points is observed, especially for equivalence ratios above $\phi \sim 0.70$.

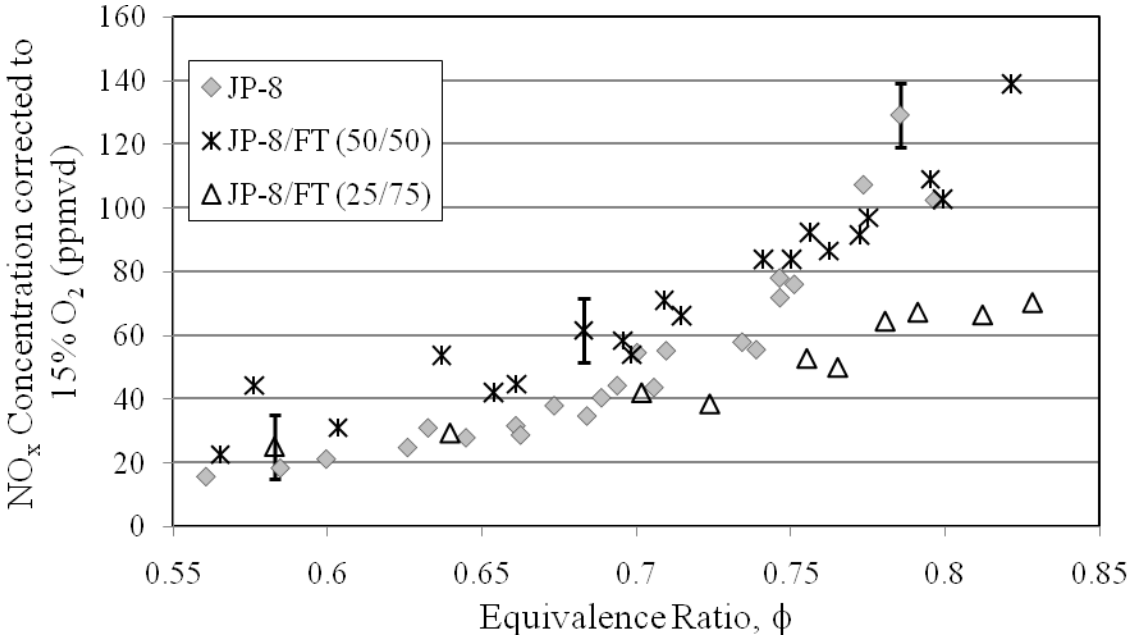

Figure 3-11 NO_x emission results for JP-8 and JP-8/FT blends as a function of equivalence ratio (2 runs of JP-8 and JP-8/FT (50/50) are presented together)

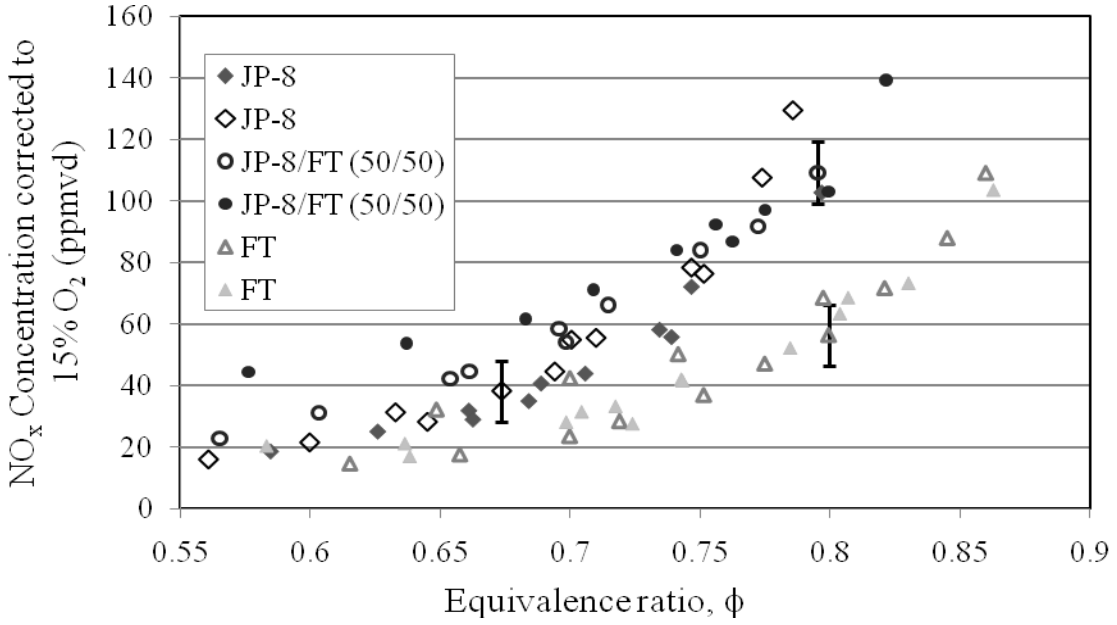

Figure 3-12 NO_x emission results for JP-8, JP-8/FT (50/50), FT fuels as a function of equivalence ratio

3.2.4.2 CO Emissions

The CO emission results for all fuels and blends are presented in Figure 3-13. The ordinate in this figure represents the CO concentration in ppm and the abscissa represents the equivalence ratio. All the CO emissions reported are corrected to 15% O_2 level. Note that FT, JP-8 and JP-8/FT (50/50) runs are repeated to compare the reproducibility of the results. To simplify the interpretation of these results, the data presented in Figure 3-13 is segregated and presented in three additional figures.

From Figure 3-13, it is observed that the CO emission results for all fuels and blends are below 50 ppm for equivalence ratios up to $\phi \sim 0.73$. Figure 3-14 presents a comparative CO emission data for JP-8, JP-900 and FT fuels. The results indicate that JP-8 produces higher amounts of CO emissions compared to JP-900 and FT. On the other hand, JP-900 shows CO emission trend analogous to FT up to an equivalence ratio of $\phi \sim 0.78$ however, above this equivalence ratio JP-900 has slightly higher CO emissions. Furthermore, a comparative representation of the CO emission results for JP-8 and JP-8/FT blends is shown in Figure 3-15. From this figure, it is clear that all fuels and blends report similar CO emission values up to an equivalence ratio of $\phi \sim 0.75$. However, for higher equivalence ratios, JP-8 shows higher CO concentrations compared to JP-8/FT (50/50) and (25/75) blends. In fact, it can be observed that the amount of CO produced reduces as the FT percentage increases, which indicates that blending FT with JP-8 can reduce CO emissions.

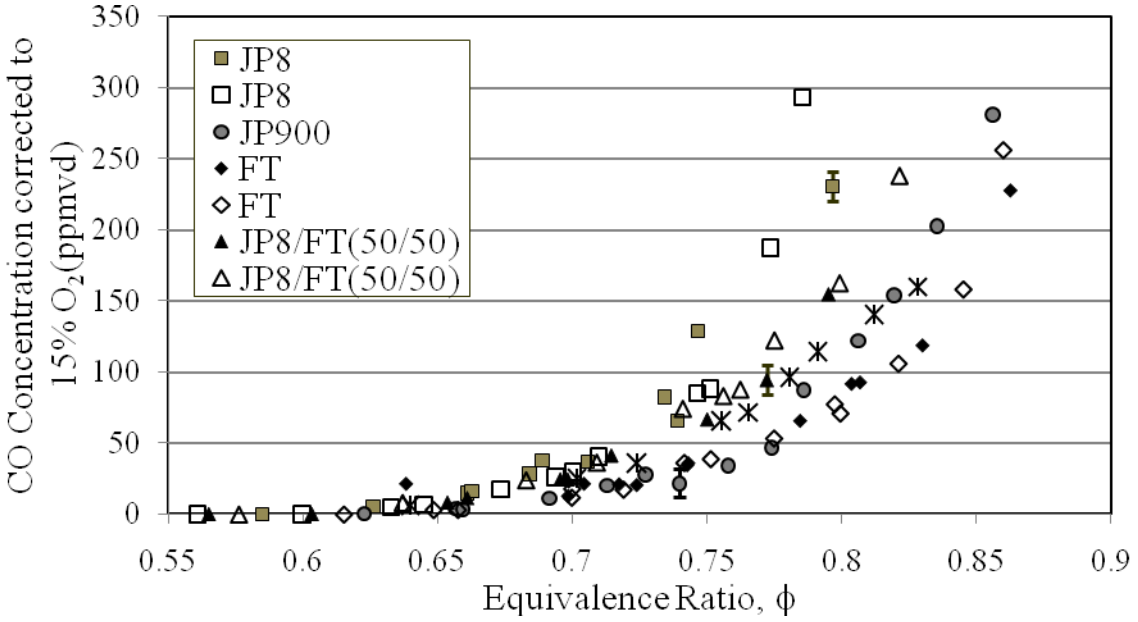

Figure 3-13 CO emission results for different fuels and blends as a function of equivalence ratio

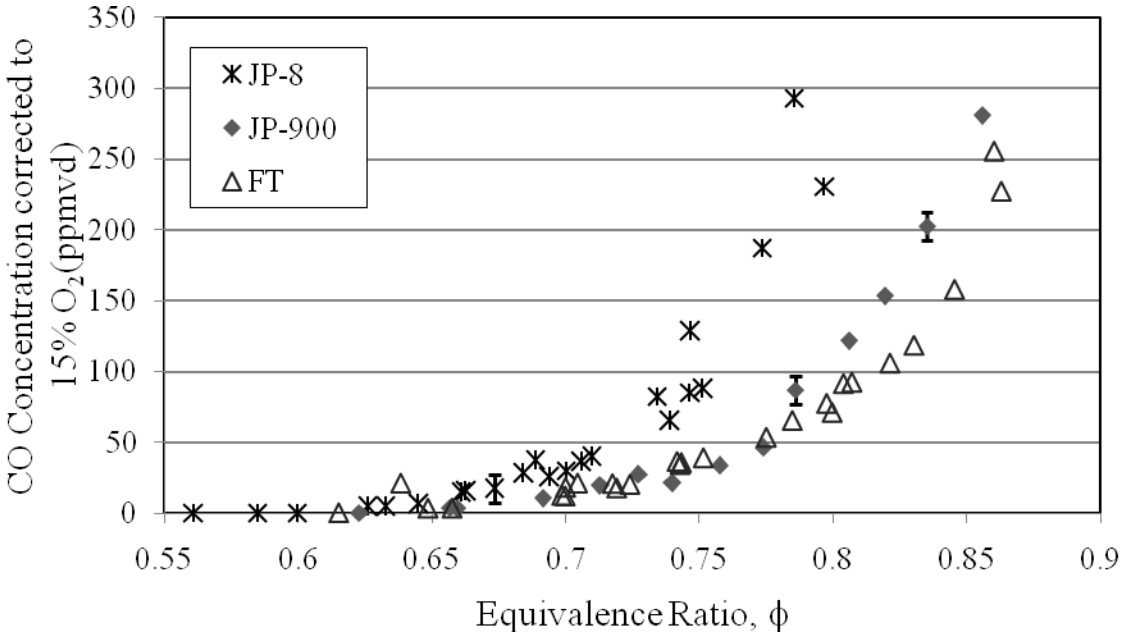

Figure 3-14 CO emission results for JP-8, JP-900 and FT fuels as a function of equivalence ratio (2 runs of JP-8 and FT are presented together)

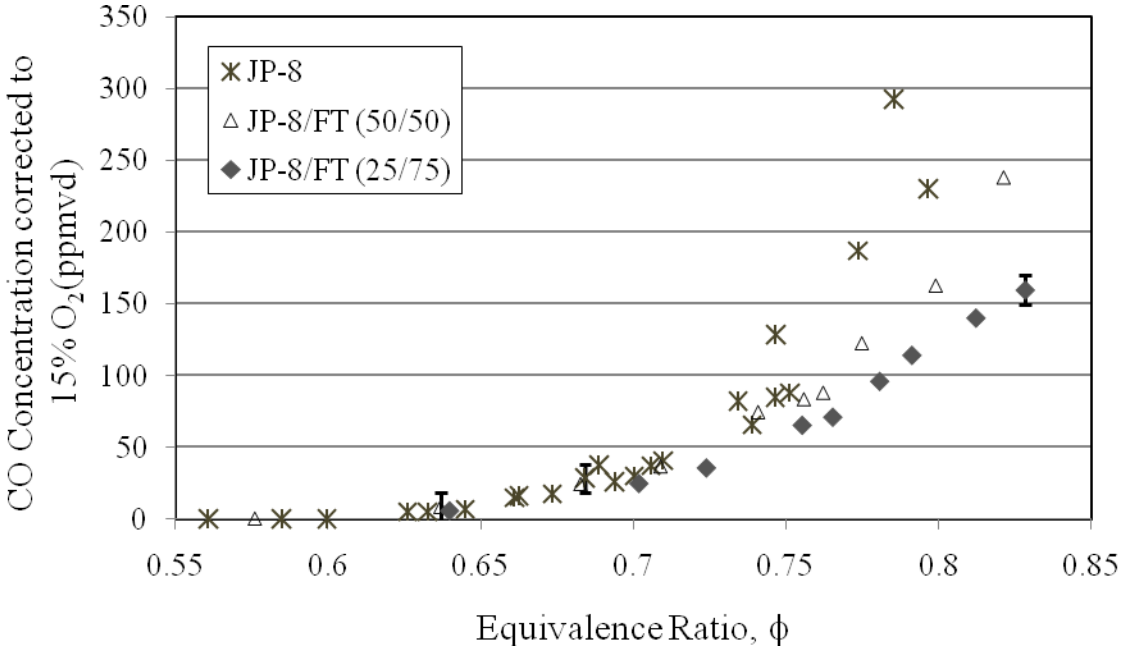

Figure 3-15 CO emission results for JP-8 and JP-8/FT blends as a function of equivalence ratio (2 runs of JP-8 and JP-8/FT (50/50) are presented together)

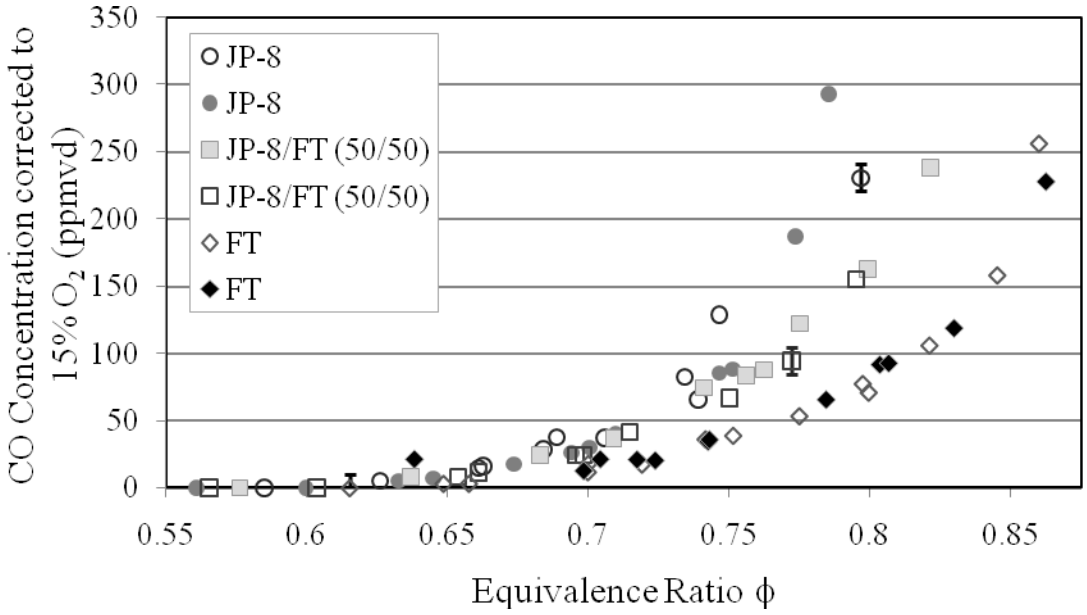

Figure 3-16 CO emission results for JP-8, JP-8/FT (50/50) blend and FT fuel as a function of equivalence ratio

Figure 3-16 shows the repeatability results for CO emission acquired for JP-8, JP-8/FT (50/50) and FT fuels. It can be observed for JP-8 that there exists a considerable scatter in measurements, especially at equivalence ratios higher than $\phi \sim 0.75$ considering the instrumentation uncertainty, which is indicated using error bars in the figure. It is observed that JP-8/FT (50/50) blend and FT fuel indicate good repeatability as compared to JP-8 and most of the data points lie within the instrumentation uncertainty. At present the anomalous results for JP-8 are not fully understood.

3.2.5 Discussion of Emission Measurements

The results presented above for the emission of NO_x and CO do present some points that warrant discussion. The fact that JP-8 and JP-8/FT (50/50) blend have high CO and NO_x emissions for equivalence ratios between $\phi = 0.7$ and $\phi = 0.9$ is perplexing. Typically, as the equivalence ratio approaches 1, the CO emissions drop while the NO_x increases sharply. The reason for both of these observations is the higher temperature, which results in faster oxidation of CO to CO_2 and the increased formation of NO_x through the Zeldovich mechanism.

Clearly, the results for CO and NO_x at higher equivalence ratios in lean region require further investigation. The higher CO concentrations may be due to incomplete combustion as a result of poor mixing or improper spray atomization and droplet distribution effects.

Chapter 4

Conclusions and Future work

4.1 Conclusions

A series of combustion studies were performed on JP-8, JP-900, FT, and 50/50, 25/75 blends of JP-8 and FT. Fuel H/C ratios, smoke points, heat of combustion and composition were determined. These fuels were tested in a model gas turbine combustor to determine combustor stability maps, mean soot volume fractions and, NO_x and CO emission measurements.

Fuels and blends were tested for stability in model gas turbine combustor. These results indicate that all fuels and blends burn stably with pressure fluctuations on the order of 1% with an exception of two cases, where the measured fluctuations were higher than 2%; however, no discernable trend was observed. In order to use these fuels and blends, they should also be tested in actual combustors to corroborate this experimental data, since instability is a function of combustor geometry and as discussed earlier, other factors like air inlet temperatures, spray patterns and fuel-air mixing characteristics also affect it.

Results of soot volume fraction measurement show that JP-8, JP-900, JP-8/FT (50/50) and (25/75) blends show a notable rise in soot volume fraction above $\phi = 1.05$ although FT fuel tends to produce lower soot over the range of equivalence ratios tested. The smoke point measurements and the estimated TSI values also suggest that FT fuel has lower tendency to produce soot. Additionally, it is also observed that the amount of

soot produced is inversely proportional to the percentage of FT in JP-8/FT mixtures. Furthermore, JP-900 has reduced soot volume fraction compared to JP-8. From these results, it is also observed that the difference in the aromatic content in fuels, as determined by the GC-MS results, is argued to be one of the reasons for higher sooting tendency of JP-8.

NO_x emission trends of FT, JP-900 and JP-8/FT (25/75) blend indicate lower values than that of JP-8 and JP-8/FT (50/50) blend. CO emissions results also show analogous trends. The JP-8 and JP-8/FT (50/50) blends show higher CO concentrations compared to FT and JP-900. Another important observation is that the amount of CO emissions reduces as the percentage of FT increases in JP-8/FT blends.

From the combustion studies results summarized above, it is observed that FT fuel shows lower propensity to form soot and exhibits NO_x and CO emissions equal to or lower than JP-8. However, as mentioned earlier, with regards to seal swell and fuel lubricity, FT cannot be used in current combustion devices. In contrast, JP-8/FT (25/75) and (50/50) blends have been shown to meet the current jet fuel specification [10] along with good seal swelling characteristics due to introduction of aromatic content from JP-8. These blends also show comparable emission characteristics, stable combustor operation and lower soot volume fractions compared to JP-8 in model gas turbine combustor. This leads to assertion that these blends could prove to be good alternatives to the existing jet fuels. Similarly, JP-900 has also shown comparable emission characteristics, stable combustor operation and lower mean soot volume fraction as compared to JP-8 in model gas turbine combustor, thus, making it a good candidate jet fuel.

4.2 Suggestions for Future Work

The current study presents a comparative study between JP-8 and other coal-based fuels, although there are areas which require further exploration. One of the major concerns during this research has been the Delavan pressure atomizer, which is exposed to high temperatures at equivalent ratios of $\phi > 0.75$. In gas turbine combustion the nozzle is a critical component that determines the effectiveness of fuel/air mixing. Any change in the spray pattern of the nozzle can impede the reproducibility of the data. In the current setup, the nozzle is situated very close to the flame and exposed to high flame temperatures, which could possibly result in coking of the fuel in the nozzle. Therefore, a change in the injection location to a position further upstream of the dump plane should be considered to avoid the nozzle from being exposed to higher temperatures. Another alternative would be to develop or procure an air-blast nozzle with higher efficiency, lower maintenance and longer life.

Modern-day gas turbine engines have higher operating pressures and temperatures. It would be noteworthy to run the same set of fuels at higher pressures and inlet temperatures and compare the results with the current study. It is expected that, the CO emissions would reduce with higher flame temperatures and thermal NO_x would increase, especially at higher equivalence ratios with the increase in adiabatic flame temperatures. Additionally, JP-900 could be pre-stressed to higher temperatures before injecting it into the combustor to determine the effects of preheat on its combustion characteristics and its resistance to coking as it is expected to show higher thermal stability.

Bibliography

1. "Effect of Fuel Structure on Pathways to Soot." Frenklach, M., Clary, D. W., Gardiner, W. C., Stein, S. E. 1988, Twenty-First Symposium (International) on Combustion/ The Combustion Institute, pp. 1067-1076.

2. "Soot in Flames and Interstellar dust." Frenklach, M., Feigelson, E.D. 1989, Earth and Mineral Sciences, Vol. 58, pp. 25-33.

3. Turns, S. R. "An Introduction to Combustion: Concepts and Applications." New York : McGraw-Hill, 2000.

4. Lefebvre, A. H. "Gas Turbine Combustion." Philadelphia : Taylor and Francis, 1989.

5. "Influence of Fuel Drop Size and Combustor Operating Conditions on Pollutant Emissions." Rink, K. K., Lefebvre, A. H. 1989, International Journal of Turbo and Jet Engines, Vol. 6(2), pp. 113-122.

6. "Dual Fuel Issues Related to Performance, Emissions, and Combustion Instability in Lean-Premixed Gas Turbine Systems." Mordaunt, C.J. 2005, Phd. Thesis, The Pennsylvania State University.

7. "Challenges and Progress in Controlling Dynamics in Gas Turbine Combustors." Mongia H. C., Held, Hsiao G. C., Pandalai R. P. 2003, Journal of Propulsion and Power, Vol. 19(5), pp. 822-827.

8. "Combustion Dynamics and Instabilities: Elementary Coupling and Driving Mechanisms." Ducruix, S., Schuller, T., Durox, D., and Candel, S. 2003, Journal of Propulsion and Power, Vol. 19(5), pp. 722-734.

9. "Fuel-Cooled Thermal Management for Advanced Aeroengines." He Huang, Spadaccini, L.J., Sobel, D.R., ASME, 2002, ASME Paper GT-2002-30070, Vol. 126, pp. 367-376.

10. "Properties and Usage of Air Force Fuel: JP-8." Edwards, T., Harrison, W.E., and Maurice, L.Q. 2001, Proceedings of the AIAA Aerospace Sciences Meeting & Exhibit, Vol. 39, pp. 1-11.

11. "Update on the Development of JP-8+100." Edwards, T., Harrison, B., Zabarnick, S., DeWitt, M., Bentz, C. E. 2004, 40th AIAA/ASME/SAE/ASEE Joint Propulsion Conference and Exhibit.

12. “Advancements in Gas Turbine Fuels From 1943 to 2005.” Edwards, T. ASME, 2007, Journal of Engineering for Gas Turbines and Power, Vol. 129, pp. 13-20.

13. “Direct Liquefaction for Production of High Yields of Feedstocks for Specialty Chemicals or Thermally Stable Jet Fuels.” Burgess, C.E., Schobert, H.H. 2000, Fuel Processing Technology, Vol. 64.

14. “Development of an Advanced, Thermally Stable, Coal-Based Jet Fuel.” Balster, L.M., Corporan, E., DeWitt, M. J., Edwards, T., Ervin, J. S., Graham, J. L., Lee, S-Y., Pal, S., Phelps, D. K., Rudnick, L. R., Santoro, R J., Schobert, H. H., Shafer, L. M., Striebich, R. C., West, Z. J., Wilson, G. R., Woodward, R., Zabarnik. 2008, Fuel Processing technology, Vol. 89, pp. 364-378.

15. “Combustion Performance of Coal-Based Fuels in a Model Gas Turbine Combustor.” Lee, S.-Y., McKeand, M., Saretto, S., Pal, S., Mordaunt, C., and Santoro, R.J. 2004, American Chemical Society, Division of Petroleum Chemistry Preprints, Vol. 49(4), pp. 513-516.

16. “Emissions Characteristics of a Turbine Engine and Research Combustor Burning a Fischer-Tropsch Jet Fuel.” Corporan, E., DeWitt, M. J., Belovich, V., Pawlick, R., Lynch, A. C., Gord, J. R., and Meyer, T. R. 2007, Energy and Fuels, Vol. 21, pp. 2615-2626.

17. “Fischer-Tropsch Fuel for Use by the U.S. Military as Battlefield-Use Fuel of the Future.” Lamprecht, D. 2007, Energy and Fuels, Vol. 21, pp. 1448-1453.

18. “The Fischer-Tropsch Process - Commercial Aspects.” Dry, M.E. 1990, Catalysis Today, Vol. 6(3), pp. 183-206.

19. “Swelling of Nitrile Rubber by Selected Aromatics Blended in a Synthetic Jet Fuel.” Graham, J. L., Striebich, R.C., Myers, K. J., Minus, D. K., Harrison,W.E. 2006, Energy and Fuels, Vol. 20, pp. 759-765.

20. “Potential Additives to Promote Seal Swell in Synthetic Fuels and Their Effect on Thermal Stability.” Dirk, D. L., Gormely, R. J., Baltrus, J. P., Anderson, R. R., Zandhuis, P. H. 2008, Energy and Fuels, Vol. 22(2), pp. 1115-1120.

21. “Effects of Aromatic Type and Concentration in Fischer-Tropsch Fuel on Emissions Production and Material Compatibility.” DeWitt, M. J., Corporan, E., Graham, J., and Minus, D. 2008, Energy and Fuels, Vol. 22, pp. 2411-2418.

22. “Qualification of Sasol Semi-Synthetic Jet A-1 as Commercial Jet Fuel.” Moses, C. A., Stavinoha, L. L., Roets, P. 1997, SwRI-8531.

23. “Stabilty and Handling of Sasol Semi-Synthetic Jet Fuel.” Roets, P., Botha, J., Moses, C., Stavinoha, L. 1998. 6th International Conference on Stability and Handling of Liquid Fuels. Vol. II, pp. 789-805.

24. “Combustion Aerodynamics.” Beer, J. M., Chigier, N. A. 1972. pp. 100-135.

25. Lefebvre, A. H. “Atomization and Sprays.” : McGraw-Hill, 1989.

26. “The Role of Fuel Preparation in Low-Emission Combustion.” Lefebvre, A. H. 1995, Journal of Engineering for Gas Turbines and Power, ASME, Vol. 117, pp. 617-655.

27. “The Elusive History of the Refractive Index of Soot.” Smyth, K. C., and Shaddix, C. R. 1996, Combustion and Flame, Vol. 107, pp. 314-320.

28. “Interpretation of Optical Measurements of Soot in Flames.” Dobbins, R. A., Santoro, R. J., Semerjian, H. G. 1984, Progress in Astronautics and Aeronautics, Vol. 92, pp. 208-237.

29. “Fuel Additive Studies In a Model Gas Turbine Combustor.” Imschweiler, D. J. 2003, M. S. Thesis, The Pennsylvania State University.

30. ASTM STANDARD, D-5373-08. “Standard Test Methods for Instrumental Determination of Carbon, Hydrogen, and Nitrogen in Laboratory Samples of Coal.”

31. ASTM STANDARD, D-1322. “Standard Test Method for Smoke Point of Kerosine and Aviation Turbine Fuel.”

32. “A Study of Sooting Tendency of Jet Fuels.” Mensch, A. 2008, M.S. Thesis, The Pennsylvania State Universtiy.

33. ASTM STANDARD, D-240-07. “Standard Test Method for Heat of Combustion of Liquid Hydrocarbon Fuels by Bomb Calorimeter.”

34. “Combustion Instability Studies in a High- Pressure Lean-Premixed Model Combustor Under Liquid Fuel Operation.” Mordaunt, C., Brossard, C., Lee, S. -Y., Santoro, R. J. 2001. Proceedings of International Joint Power Generation Conference, ASME.

35. “Liquid Propellant Rocket Combustion Instability.” Harrje, D. T., Reardon, F. H. 19, 1972, NASA SP-194.

36. “Experimental Study of Fuel Decomposition and Hydrocarbon Growth Processes for Cyclohexane and Related Compounds in Non Premixed Flames.” McEnally, C. S., Pfefferle, L. D. 2004, Combustion and Flame, Vol. 136, pp. 155-167.

37. “Experimental Study of Fuel Decomposition and Hydrocarbon Growth Processes for Practical Fuel Components: Heptanes.” McEnally, C. S., Ciuparo, D. M., Pfefferle, L. D. 2003, Combustion and Flame, Vol. 134, pp. 339-353.

38. “Describing the Uncertainties in Experimental Results.” Moffat, R.J. 1998, Experimental Thermal and Fluid Science, Vol. 1, pp. 3-17.

Appendix A

Uncertainty Analysis

Results obtained in an experiment may not represent the exact values and there always exists some uncertainty in the measurements made. Uncertainty analysis helps in determining the possible value of error associated with regards to measured quantities [6].

A.1 Method of Uncertainty Analysis

Given a desired result, R, which is expressed as:

$$R=R(x_1, x_2 \ldots x_n) \tag{A.1}$$

where x_i represents an independent variable, the uncertainty of the result, δR, can be expressed as:

$$\delta R = \left[\left(\frac{\partial R}{\partial x_1} \delta x_1 \right)^2 + \left(\frac{\partial R}{\partial x_2} \delta x_2 \right)^2 + \ldots + \left(\frac{\partial R}{\partial x_n} \delta x_n \right)^2 \right]^{1/2} \tag{A.2}$$

Where δx_i indicates the uncertainty associated with each independent variable. Sometimes it is possible to express R in a product form as [38]:

$$R = x_1^a x_2^b \ldots x_n^m \tag{A.3}$$

The corresponding uncertainty can then be expressed as:

$$\frac{\delta R}{R} = \left[\left(a \frac{\delta x_1}{x_1} \right)^2 + \left(b \frac{\delta x_2}{x_2} \right)^2 + \ldots + \left(m \frac{\delta x_n}{x_n} \right)^2 \right]^{1/2} \tag{A.4}$$

A.2 Uncertainty Estimation for Metering and Measuring Instruments

Table A-1 shows typical values for instrumentation range and accuracies used in the model gas turbine combustor system.

Table A-1 Typical range and accuracy of instrumentation used on model gas turbine combustor

Instrument	Range	Accuracy
K-type thermocouples	273 K – 1523 K	$\pm$ 2.2 K
Setra Pressure transducers	0-1000 psia	$\pm$ 0.11 % F.S
Setra Pressure transducers	0-2000 psia	$\pm$ 0.11 % F.S
Setra Pressure transducers	0-3000 psia	$\pm$ 0.11 % F.S
Piezo electric pressure transducers	0-200 psia	$\pm$ 1.00 % F.S
Hoffer flow meter	0.5-9.5 mL/s	$\pm$ 0.05 % F.S

Venturi	C_D	C_D Uncertainty
Fox jewel orifice D = 0.762 mm	0.9122	$\pm$ 1.0 %
Inlet Air orifice D = 3.81 mm	0.9710	$\pm$ 2.5 %

Using the above method, uncertainties for critical components of the system are calculated and shown in Table A-2.

Table A-2 Calculated uncertainties of critical quantities

Parameter	Uncertainty value
Static pressure δP	$\pm$ 3.3 psia
Dynamic Pressure $\delta P'$	$\pm$ 0.013psia
Temperature δT	$\pm$ 2.2 K
Gaseous Fuel equivalence ratio $\delta\phi/\phi$	$\pm$ 2.80 %
Liquid Fuel equivalence ratio $\delta\phi/\phi$	$\pm$ 2.60 %

Appendix B

Other Experimental Results

B.1 CNG Emission Results

As mentioned earlier, CNG measurements were obtained before and after the liquid fuel tests in order to determine the calibration drifts in emission analyzers. These measurements for NOx and CO emissions are presented in Figure B-1 and Figure B-2 respectively.

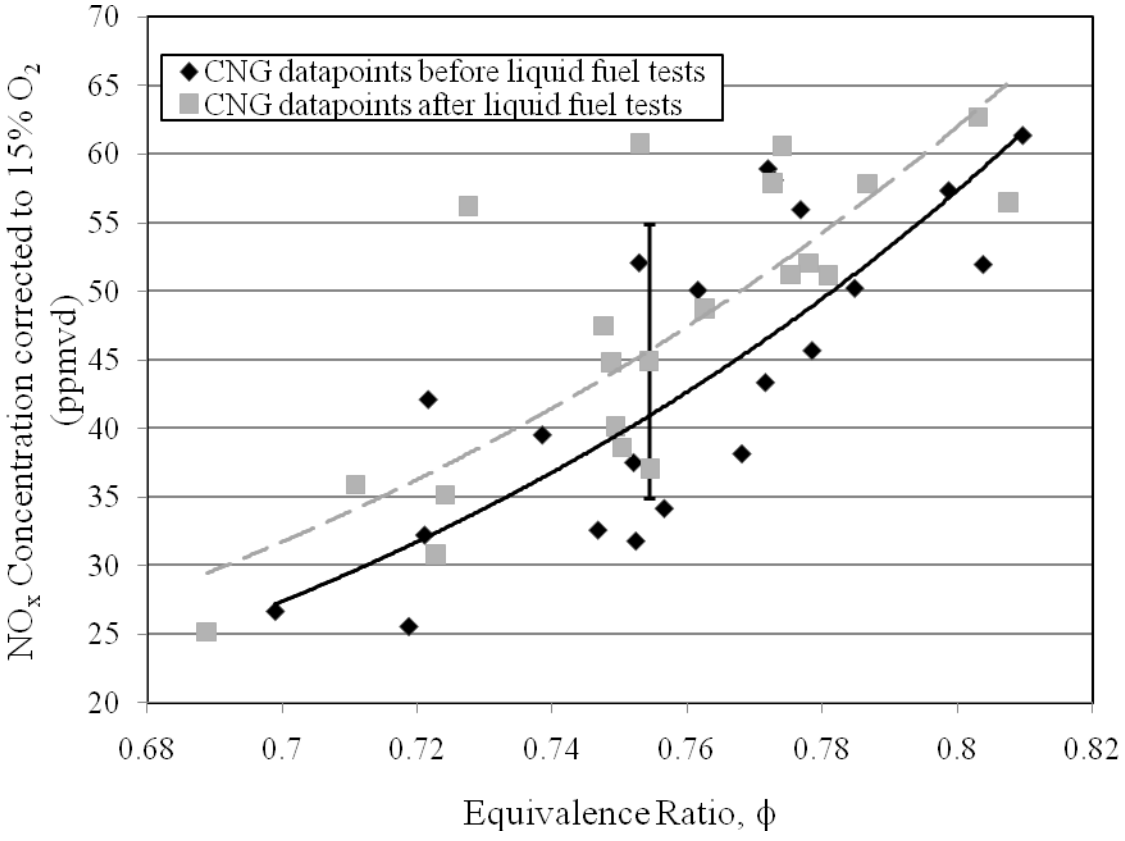

Figure B-1 NO_x emission for compressed natural gas as a function of overall equivalence ratio

The analyzers were also calibrated using accurate calibration gases before the test and this calibration was tested at the end of the experiment. These CNG data points do support these calibration tests done before and after the experiment. The reasons for calibration drift of analyzers can be a choked filter used to filter out PM from the exhaust gases, drifting caused by change in instrumentation temperature, etc.

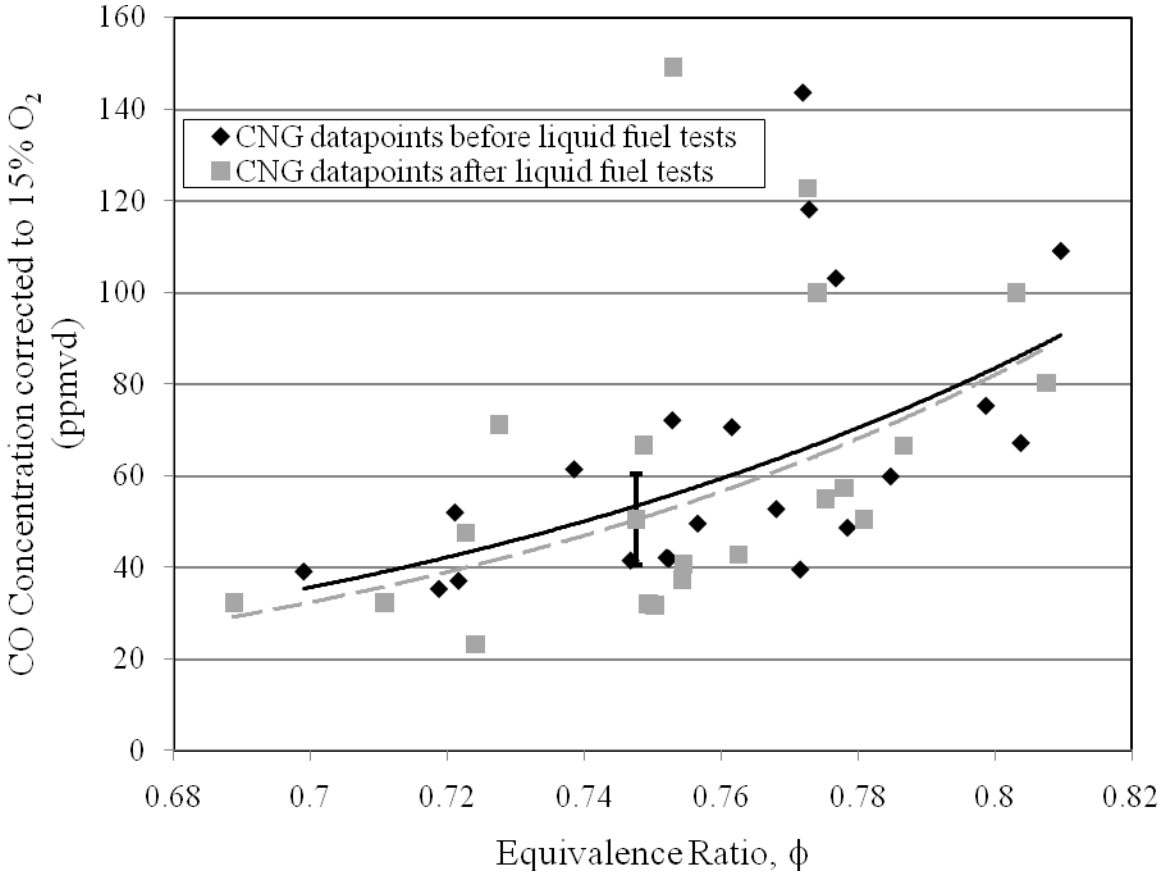

Figure B-2 CO emission results for compressed natural gas as a function of overall equivalence ratio

Figure B-1 shows NO_x measurements for CNG data points at different equivalence ratios obtained before and after the liquid fuel experiment for all the fuels

tested. The ordinate in this figure represents the NO_x concentration in ppm and the abscissa represents the equivalence ratio. The dashed line represents the trend line for CNG data points obtained after the liquid fuel experiments and the solid line represents the trend line for CNG data points obtained before the liquid fuel experiments. As seen from the figure, most of the CNG points fall within the NO_x analyzer instrumentation error. It can be concluded that the results obtained for liquid fuels indicate true values that lie within the instrumentation uncertainty.

In Figure B-2, the ordinate represents the CO concentration in ppm and the abscissa represents the equivalence ratio and similar to Figure B-1, the dashed and the solid trend lines correspond to CNG data points after and before the liquid fuel experiments respectively. Although, in Figure B-2 there are some points for the JP-900 and JP-8 tests, which indicate a higher value of CO. These points fall outside the general trend of most of the scattered points; however, these discrepancies have no discernable trend and no notable changes in calibration were observed for these runs at the end of the experiment. Hence similar to NO_x results it can be concluded that the values obtained for CO emission of liquid fuel experiments correspond to true values that lie within the instrumentation uncertainty.